Mathematical Models for 3-Phase Traffic Flow Theory

Vom Fachbereich Mathematik
der Technischen Universität Kaiserslautern
zur Verleihung des akademischen Grades

Doktor der Naturwissenschaften
(Doktor rerum naturalium, Dr. rer. nat.)

genehmigte Dissertation

von
Mark Eric Mwiti Kimathi

Gutachter:	Prof. Dr. Axel Klar
	Prof. Dr. Reinhard Illner
Datum der Disputation:	14 Februar 2012

D 386

To my lady friend Ms. Asenath.

Acknowledgements

To start with, I specially thank God the almighty for His blessings, guidance and protection throughout my studies.

I profoundly thank my supervisor, Prof. Dr. Axel Klar for his superb supervision. His judicious guidance, support and encouragement effectively helped me succeed in my Ph.D. studies.

Also, I express my sincere appreciation to Prof. Dr. Reinhard Illner of the University of Victoria, Canada for serving as a reviewer of this doctoral thesis.

My gratitudes goes to the AGTM group, Technical University of Kaiserslautern, Germany for the cordial working environment. I hereby acknowledge the much help I received from Dr. Raul Borsche on issues concerning numerical schemes. I also specially thank Mr. Prabhath Liyanage, Dr. Sudarshan Tiwari and Ms. Anamika Pandey for their assistance on various matters, both academic and non-academic. Also a must mention is one Dr. Richard Avuglah, Ghana, not forgetting Dr. Anthony Waititu, Kenya, who really helped me in one way or another in achieving this academic success.

I salute my dear parents for their unwavering support, whence I state that my success means that you have succeeded in parenting. My sincere thanks are due to my brothers, sisters and, to my lady friend Ms. Asenath for their immense encouragements.

To sum up, I am so grateful to the German Academic Exchange Service (DAAD) for the award of a PhD scholarship in the "Mathematics in Industry and Commerce" program and also the financial support I received from the Technical University of Kaiserslautern.

Abstract

In this thesis we outline the Kerner's 3-phase traffic flow theory, which states that the flow of vehicular traffic occur in three phases i.e. free flow, synchronized flow and wide moving jam phases. A macroscopic 3-phase traffic model of the Aw-Rascle type is derived from the microscopic Speed Adaptation 3-phase traffic model developed by Kerner and Klenov [*J. Phys. A: Math. Gen., 39(2006), pp. 1775–1809*]. We derive the same macroscopic model from the kinetic traffic flow model of Klar and Wegener [*SIAM J. Appl. Math., 60(2000), pp. 1749–1766*] as well as that of Illner, Klar and Materne [*Comm. Math. Sci., 1(2003), pp. 1–12*]. In the above stated derivations, the 3-phase traffic theory is constituted in the macroscopic model through a relaxation term. This serves as an incentive to modify the relaxation term of the 'switching curve' model of Greenberg, Klar and Rascle [*SIAM J. Appl. Math., 63(2003), pp.818–833*] to obtain another macroscopic 3-phase traffic model, which is still of the Aw-Rascle type. By specifying the relaxation term differently we obtain three kinds of models, namely the macroscopic Speed Adaptation, the Switching Curve and the modified Switching Curve models. To demonstrate the capability of the derived macroscopic traffic models to reproduce the features of 3-phase traffic theory, we simulate a multilane road that has a bottleneck. We consider a stationary and a moving bottleneck. The results of the simulations for the three models are compared.

Zusammenfassung

Die vorliegende Arbeit befasst sich mit Kerners 3-Phasen Verkehrsmodellen, in denen der Verkehrsfluss in drei Phasen betrachtet wird, *free flow, synchronized flow* und *wide moving jams*. Zu Beginn wird ein makroskopisches 3-Phasen Modell vom Aw-Rascle Typ aus dem mikroskopischen *Speed Adaptation* von Kerner und Klenov entwickelt [*J. Phys. A: Math. Gen., 39(2006), pp. 1775–1809*]. Das selbe Modell kann von den kinetischen Verkehrsmodellen von Klar und Wegener [*Comm. Math. Sci., 1(2003), pp. 1–12*] sowie Illner, Klar und Materne abgeleitet werden [*Comm. Math. Sci., 1(2003), pp. 1–12*]. In diesem neuen makroskopischen Modell wird die 3-Phasen Verkehrstheorie als Relaxationsterm berücksichtigt. Ein ähnliches Verkehrmodell kann aus dem '*switching curve*' Modell von Greenberg, Klar und Rascle [*SIAM J. Appl. Math., 63(2003), pp.818–833*] durch eine Anpassung des Relaxationsterms hergeleitet werden. Des Weiteren wird ein drittes Modell, das *modified Switching Curve model*, als Übergang zwischen den beiden vorherigen konstruiert. Das Verhalten dieser drei Modelle wird anhand von mehreren numerischen Beispielen untersucht. Alle drei Phasen des Verkehrsflusses können bei Fahrbahnverengungen beobachtet werden. Hierbei werden auch bewegliche Fahrbahnverengungen betrachtet.

Contents

1 Introduction

1.1 Overview

Congestion of vehicular traffic within urban areas is a problem experienced worldwide. It has adverse effects on people quality of life due to delays, accidents and environmental pollution. One way of eliminating the problem is to increase the capacity of existing roadways by addition of lanes. However, this is greatly hampered by lack of space, resources or due to environmental issues and sometimes politics. This leaves the relevant authorities with one major option, that of enhancing the utilization of existing infrastructure by employing better traffic management and operations strategies. For effective traffic management and control, proper understanding of traffic congestion is needed. To achieve the latter, spatiotemporal behavior of empirical traffic congested patterns should be studied closely. This is because traffic congestion is observed to take place in space and time in form of spatiotemporal congested traffic patterns that propagate within roadways. Empirical observation indicate that traffic congestion in a road network is a consequence of traffic breakdown in initially free flowing traffic [1]. Traffic breakdown is the abrupt decline of velocity from high values in free flow to lower values in congested traffic, and normally happens at highway bottlenecks such as on-and off-ramps, lane-drops, accidents etc.

Now that the origin of traffic congestion is known, it is essential to adequately describe the situations which are the origin of congestion on road networks. This calls for traffic flow theories and models whose objective is to describe in a precise mathematical way the vehicle to vehicle interactions and interactions between vehicles and infrastructure. One such theory is the 3-phase traffic theory since it was developed to explain traffic breakdown and the resulting spatiotemporal features of congested vehicular traffic, see [1]. As a remark, it was illustrated by Kerner in [1] that earlier traffic flow theories fail to explain the real cause of traffic congestion i.e. traffic breakdown, and many of the resulting spatiotemporal congested traffic patterns. This failure is attributed to the fact that these traffic flow theories and models are based on the fundamental diagram of traffic flow which states that there exists a correspondence between a given value of traffic density and the flow rate for all density values in the range $[0, \rho_{max}]$, where ρ_{max} is the maximal density. An account of various mathematical models based on the fundamental diagram of traffic flow can be found in [39] among others. These models can be categorized as

microscopic, macroscopic and mesoscopic traffic flow models. Microscopic models entails the tracking of every vehicle to describe its behavior and interactions with other vehicles in traffic stream. Macroscopic models describe traffic flow dynamics in an aggregate manner using characteristics such as density, velocity and flow rate. Mesoscopic model(kinetic models) describe traffic flow in less aggregate manner than macroscopic models and in probabilistic terms. Microscopic traffic flow models based on 3-phase traffic theory already exists, see [1, 3, 25, 26]. However, there are hardly any macroscopic traffic flow models within the 3-phase traffic theory framework. This brings us to the following objective of this study.

The main aim of this study is to develop a macroscopic traffic flow model that is based on 3-phase traffic theory. To do this, we utilize a relaxation term to institute the 3-phase traffic flow theory, emulating what was done in the microscopic 3-phase traffic models developed in [3]. All the while we ensure that the macroscopic model satisfies the anisotropic property of traffic flow, see [9], by using appropriate transformations and approximations in the derivation of the macroscopic traffic models from microscopic and kinetic traffic models. Another objective is to employ suitable numerical methods to solve the macroscopic model equations so as to ensure the model features are preserved while simulating traffic breakdown and the resulting spatiotemporal congested traffic patterns.

Some parts of this thesis have been presented in [40] and [41].

1.2 Structure of the Study

In Chapter 2 we outline the Kerner's 3-phase traffic flow theory [1] by stating the three traffic phases that comprise this theory; namely free flow, synchronized flow and wide moving jams. The factors prompting the first order transitions from one phase to the other are also presented. Moreover, the significance of space gaps in explaining 3-phase traffic theory is stated. The chapter is closed with an account of microscopic mathematical models developed in [1, 3, 25, 26] for 3-phase traffic flow and give a highlight of the attributes to failure of macroscopic traffic models in explaining 3-phase traffic flow features. We also mention the claim made by Helbing and co-workers [21, 28] in as far as spatiotemporal congested traffic patterns are concerned.

The derivation of macroscopic 3-phase traffic flow models is devoted to Chapter 3. We begin by deriving the model from the microscopic Speed Adaptation 3-phase traffic model [3], then from kinetic traffic flow models [6, 38] and lastly from the macroscopic Switching Curve model [14] whilst constituting the 3-phase traffic theory in the models through a relaxation term. The chapter is concluded by studying the structural properties of the derived macroscopic models and with a presentation of the solution to the Riemann problem set up using the conservative form of this

Aw-Rascle type traffic model.

Chapter 4 presents the numerical solution to the derived macroscopic models. In this chapter we outline the Godunov scheme and point out its inadequacy in resolving contact discontinuity, which is a solution to the Riemann problem set up using the above stated traffic model. What follows is an algorithm, proposed in [16], that remedies the above stated deficiency of the Godunov scheme. This algorithm involves the use of the Godunov scheme to approximate shocks and rarefaction waves and applies a Glimm's random sampling technique to resolve contact discontinuities with infinite resolution. By simulations we demonstrate the capability of the derived macroscopic traffic models to reproduce the features of 3-phase traffic theory such as traffic breakdown and $F \rightarrow S \rightarrow J$ phase transitions. This is done for a stationary and a moving bottleneck.

2 The 3-Phase Traffic Flow Theory

2.1 3-Phase Traffic Theory Hypothesis

The 3-phase traffic theory (3-PTT) is an alternative traffic flow theory introduced by Kerner [1] to explain the empirical spatiotemporal features of vehicular traffic. The use of the term spatiotemporal is justified by the fact that, in reality, traffic occurs in space and time. According to Kerner, a traffic phase is a state of traffic viewed in space and time and found to posses some unique empirical spatiotemporal features. Usually traffic is considered to be in free flow state or in congested state. However a closer examination of the congested traffic in space and time reveals that there exists two different phases i.e. synchronized flow and wide moving jams. Hence the 3-PTT comprises of three traffic phases, namely: free flow (F), synchronized flow (S) and wide moving jams (J).

As the name suggests, in free flow traffic phase the vehicles move freely with negligible vehicle to vehicle interactions and therefore they have an opportunity to move with their desired maximum speeds, unless restricted by the traffic regulations. This occurs when the vehicle density in the traffic stream is small. The free flow (F) phase reigns but as the density increases, leading to an increase in the flow rate, a limit for this phase existence is reached since the vehicle interactions, that can no longer be neglected, result in a decrease of the average vehicle speeds. This limit point of free flow occurence denotes the maximum values to which the density and flow rate can increase and at which the probability of a phase transition to a congested traffic phase is equal to one [19].

To identify the difference between synchronized flow and wide moving jams, we begin by defining the latter. A wide moving jam (J) is a localized congested traffic feature with a high vehicle density and low velocity that propagates upstream in traffic, which is normally flowing downstream. It is a localized structure in the sense that it is spatially restricted by two jam fronts i.e. the downstream and the upstream jam fronts such that within the downstream jam front vehicles accelerate from the low velocity inside the jam to higher velocity in traffic flow downstream of the jam; whereas within the upstream jam front, the vehicles decelerate to the low velocity inside the jam. The two jam fronts move upstream and thus this gives the wide moving jam its distinctive feature of propagating through any states of free flow and synchronized flows and even through any bottleneck such as on/off-

ramps while maintaining the mean velocity of the downstream jam front of between negative 14-20 km/h [20].

Synchronized flow (S) is any congested traffic that does not exhibit the above distinctive feature of wide moving jams. In particular the downstream jam front is often fixed at the bottleneck. In the case that synchronized flow happens to move, the mean velocity of the downstream front changes in a wide range during the pattern propagation. Another notable feature of synchronized flow is the formation of diverse spatiotemporal traffic patterns uptream of the bottleneck. This leads to the following types of synchronized flow patterns (SP) [1]: localized SP (LSP), widening SP (WSP) and moving SP (MSP). A LSP is whereby the downstream front of the SP is fixed at the bottleneck and the upstream front propagates upstream (but not continuously) in the course of time only to get localized at some distance upstream of the bottleneck. The WSP is whereby the downstream front is fixed at the bottleneck, just like the LSP, but the upstream front continuously propagate upstream in the course of time. The WSP can also be termed as SP of higher vehicle speed in the case that the bottleneck influence on the highway is relatively low. An MSP can be realized when both upstream and downstream fronts of a SP propagate upstream on the road for as long as it does not encounter another bottleneck upstream where it is likely to induce traffic breakdown(see [1] for more discussion). Basically, MSP and narrow moving jam are all the same thing if a propagating narrow moving jam is sorrounded both upstream and downstream by free flow.

2.1.1 Phase Transitions in Traffic Flows

The motivation of distinguishing congested traffic as synchronized flow (S) and wide moving jams (J) is to have a proper understanding of the common spatiotemporal features of congested traffic patterns, which are the origin of the hypotheses of 3-PTT, with the objective of deducing effective and reliable traffic control and management strategies. It has been observed that traffic congestion occurs mostly in the vicinity of highway bottlenecks such as on/off-ramps, lane-drops, workzones, road gradients, accidents e.t.c. Therefore, if on many different days traffic flow frequently breaks down or congestion sets in at a certain highway bottleneck, then this bottleneck is termed as an *effectual bottleneck*[1]. The common spatiotemporal features of congested traffic are affiliated with the behaviour of the downstream front of a congested traffic pattern at an effectual bottleneck, at which onset of congestion is likely to happen. A term used to describe the nature of traffic congestion emergence at bottlenecks is traffic breakdown. Thus *traffic breakdown* is termed as the onset of congestion in an initially free flow traffic whereby there is an abrupt decrease in vehicles average velocity in free flow to a considerably lower velocity in congested traffic. Upon the occurence of traffic breakdown, the ensuing spatiotemporal congested pattern often has its downstream front fixed at the effectual bottleneck

location. Therefore, traffic breakdown is associated with the $F \rightarrow S$ phase transition. Other fundamental features of traffic breakdown are: at a bottleneck, it can occur spontaneously or be induced by a spatiotemporal congested traffic pattern propagating from another bottleneck situated downstream, secondly, this onset of congestion and its dissolution is accompanied by a hysteresis effect, and thirdly, traffic breakdown exhibits a probabilistic nature,see [1].

Having indicated how the $F \rightarrow S$ phase transition comes about, we now look at how wide moving jams emerge in synchronized flow i.e. $S \rightarrow J$ phase transition. The advocacy of Kerner's 3-PTT is that wide moving jams do not emerge spontaneously in free flow. Therefore they can only emerge spontaneously in synchronized flow phase, as has been observed in real measured traffic data. It has been empirically found out that this $S \rightarrow J$ transition is associated with a pinch effect in synchronized flow [23, 24]. *Pinch effect* is the spontaneous emergence of a growing narrow moving jam in synchronized flow whereby the average density increases and average velocity decreases significantly, however, the average flow rate can be great. The emergence of growing narrow moving jams in metastable synchronized flow can be caused by unexpected braking of a vehicle in synchronized flow, lane changing and merging of vehicles from other roads thus causing fluctuations in the traffic flow variables. Usually $S \rightarrow J$ transition occurs upstream of the bottleneck location and also upstream of the road location where the growing narrow moving jam has initially appeared. The latter is because there is a time lapse for this moving narrow jam to grow into a wide moving jam.

Nevertheless, Helbing and co-worker [21] seriously question 3-PTT validity basing their arguments on empirical data from the German freeway A5 close to Frankfurt, which is the same stretch of freeway from which most of the observations were done that led to development of 3-PTT. They take issue with the classification of congested traffic states as moving synchronized pattern and wide moving jams, preferring not to distinguish between them and just refer to them as moving jams. They also argue that the general pattern (which is as a result of wide moving jam emergence in synchronized flow) is a congested traffic pattern not arising from an isolated bottleneck but rather arises due to a combination of one or many on-ramps with one or many off-ramps situated upstream of the on-ramp(s).

2.1.2 Space Gaps as an Impetus to Traffic Breakdown

Many traffic operations such as lane-changes, merging of vehicles at on-ramps, and crossing at intersections depend on the availability of space gaps (i.e. the distance between the front bumper and the rear bumper of two vehicles following one another) in traffic flow. Sullivan and Troutbeck [22] showed that space gaps are crucial in the analysis of non-signalised intersections and roundabouts. Moreover, the characteristics of space gaps is quite relevant in the study of optimal traffic signal control.

We remark that the distribution of space gaps has a significant effect on platoon formation and delays. Actually, space gaps are a basic ingredient in the Acceleration Time Delay model of three-phase traffic flow developed by Kerner and Klenov in [3]. As discussed in [1], the nature of traffic breakdown is explained by a competition of two opposing tendencies i.e. the tendency towards synchronized flow due to vehicle deceleration to adapt to the speed of the leading vehicle and the tendency towards the initial free flow due to vehicle acceleration after relieving its constrainedness through a lane-change manoeuvre to a faster lane. The tendency associated with speed adaptation effect can be described using space gaps as follows: whenever a vehicle approaches a slower preceding vehicle and cannot overtake, it decelerates to adapt its speed to the speed of the preceding vehicle at any space gap within the space gap range; see [1]:

$$h_{safe}(u) \leq h \leq h_S(u). \tag{2.1}$$

without caring what is the precise space gap to the preceding vehicle i.e. at a given steady speed in synchronized flow a driver makes an arbitrary choice of a space gap from a multitude of space gaps within the range given above. $h_S(u)$ is known as the synchronization gap and is given by;

$$h_S(u) = u\tau_s; \quad \tau_s = \tau_0 \left(1 - 0.95 \left(\frac{u}{V_{max}}\right)^2\right). \tag{2.2}$$

whereas $h_{safe}(u)$ is the safe gap and expressed in terms of the safe time gap as;

$$h_{safe}(u) = u\tau_{safe}. \tag{2.3}$$

where u is the average velocity, V_{max} is the maximum velocity and τ_0, τ_{safe} are constants. The second tendency that causes traffic breakdown at bottlenecks i.e. the one due to acceleration can be described using space gaps by considering vehicle motion on a multi-lane road occurring under the condition given by (2.1) and assuming that later the vehicle can pass the slow moving preceding vehicle by performing a lane-change manoeuvre to a faster lane and accelerating. Noting that at any given density, the probability of changing lanes is greater in free flow than in synchronized flow and that the steady states of synchronized flow cover a 2D-region in the flow-density plane, we deduce that the probability of lane-changes should be modeled in such a way that it exhibit a discontinuous character i.e. a drop in lane-change probabilities when free flow transforms into synchronized flow.

Remark 2.1.1. *A traffic state whereby (2.1) is satisfied is the so-called steady state of synchronized flow that covers 2D-region in the flow-density plane, within the framework of the three-phase traffic flow theory as shown in figure 2.1. The safe gap determines the upper boundary of the 2D-region in the flow-density plane and the synchronization gap determines the lower boundary of the 2D-region in the flow-density plane such that for $h < h_{safe}(u)$ the vehicle decelerates while for $h \geq h_S(u)$ the vehicle accelerates.*

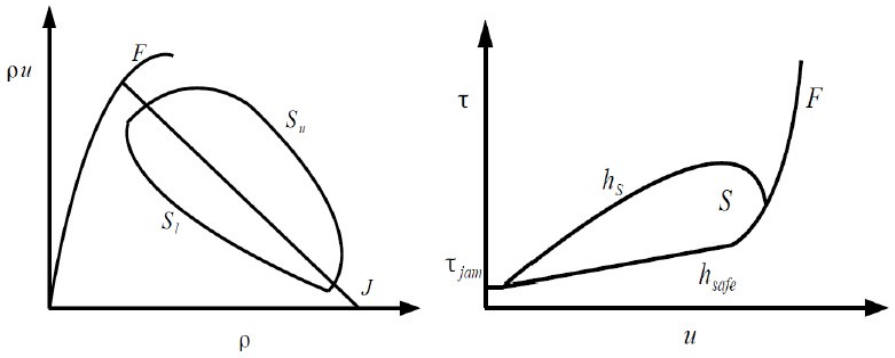

(a) (b)

Figure 2.1: The fundamental hypothesis of 3-phase traffic theory. In (a), qualitative representation of free flow (F), the 2D-region of synchronized flow (S), and the line J associated with wide moving jams in the flow-density plane. In (b), h_S is the synchronization gap that determines the lower boundary S_l and h_{safe} is the safe gap that determines the upper boundary S_u in the flow-density plane (a).

2.2 Mathematical Models for 3-Phase Traffic Flow

Microscopic 3-phase traffic flow models that can reproduce empirical features of traffic breakdown and the resulting spatiotemporal congested features, can be categorized as stochastic, deterministic and cellular automata models.

The Kerner-Klenov (K-K) stochastic 3-phase traffic model [25, 1] uses a variety of driver behavioral characteristics which significantly impact on the spatiotemporal congested traffic patterns that occur at bottlenecks. In [1] it is explained that the onset of congestion is as a result of competition between the speed adaptation effect and the over-acceleration effect that both act in an opposing manner. In the K-K stochastic model, the speed adaptation effect is achieved via a random speed change that is applied depending on whether the vehicle decelerates or accelerates. The over-acceleration effect is achieved either through a random driver acceleration, a lane change maneuvre to a faster lane or through a combination of both the lane change processes and a random driver acceleration.

The cellular automata (CA) models within the framework of 3-PTT are developed based on the Nagel-Schreckenberg ideas of traffic modeling. The major difference between the 3-phase CA traffic model [26], i.e. KKW CA model, and the earlier CA models, which are based on the fundamental diagram approach, is that the acceleration behaviour in the former model is dependent on some synchronization distance. In particular, the rule of changing velocity in this KKW CA model is given in such

a way that there is neither a velocity-dependent distance, which individual drivers would choose to drive at, nor is there a density-dependent (space gap-dependent) optimal velocity that drivers would accelerate to. Prescribing the rule of velocity change in the above stated manner, ensures that the model is able to reproduce the 2D region(in the flow-density plane) of steady states of 3-PTT. For the earlier CA models, see [26], that are not within the framework of 3-PTT, the steady states lies on a curve that is the fundamental diagram.

Remark 2.2.1. *In the steady states of synchronized flow that cover a 2D region in both the distance-velocity and flow-density planes, the velocity and distance/space-gap are integers in KKW CA model [26] but not in the stochastic K-K model [25]. However, the speed adaptation and the over-acceleration effects are simulated in the same manner (i.e. stochastically) as in the K-K model.*

Another CA model, with velocity adaptation in the 3-PTT framework, is proposed in [27]. This model is developed in such a way that the vehicle dynamical rules are randomly changed over time between the rules of the standard Nagel-Schreckenberg CA model, so as to reproduce wide moving jams, and the rules of the KKW CA model, so as to take into account the speed adaptation effect of the 3-PTT, that enables the model to show synchronized flow. See [27] for other microscopic models in the 3-PTT framework. An underlying feature of microscopic traffic flow models is that if the velocity difference between the following vehicle velocity and the velocity of the leading vehicle changes, then the follower vehicle accelerates (or decelerates) with a time delay. In stochastic and cellular automata models in the context of 3-PTT, the time delays in acceleration(or deceleration) are taken into account mainly through the use of random model fluctuations, which is not so realistic.

Hence Kerner and Klenov in [3] went ahead to develop a deterministic microscopic model still in the context of 3-PTT, namely the Acceleration Time Delay (ATD) model, that explicitly describes the driver time delays in acceleration (or deceleration). The development of this ATD model is based on empirical features of traffic phase transitions and spatiotemporal congested patterns together with some assumptions of vehicles behaviour presented therein. In the ATD model, the speed adaptation effect is modeled deterministically through a driver acceleration term whereby the driver adjusts the velocity to that of the leading vehicle within a synchronization gap. The over-acceleration effect is also deterministically modeled through a driver acceleration term whereby the driver adjusts the velocity to a predetermined space gap-dependent optimal velocity in free flow. Moreover, the emergence of moving jams in synchronized flow is simulated through the use some specified driver time delays, see [3] for details. Therein, another deterministic microscopic 3-PTT model is developed, that is the Speed Adaptation (SA) model whose major difference with the ATD model lies in how the steady states are represented on the flow-density plane. Just as in the hypothesis of 3-PTT, the steady states in the ATD model cover a 2D region in the flow-density plane, whereas in the SA

model, that is still in the context of 3-PTT, these steady states are averaged and so they cover a 1D region in the flow-density plane and are therefore represented by a curve on that plane.

Remark 2.2.2. *As pointed out by the authors, one aim of this SA model, which is a simplification of the ATD model, is to simulate the traffic phase transitions and features of congested traffic in a simpler way. Another aim is to underscore the notion that if the hypothesis of 3-phase traffic theory rather than the fundamental diagram hypothesis is to form the basis of a mathematical model for traffic flow, then that model can show and predict some (if not all) key empirical features of phase transitions in traffic flow.*

Based on the very recent discussion done by Kerner in the book [1] and on this study author's knowledge, macroscopic traffic models developed on the basis of the 3-PTT are virtually non-existent. This is because the existing macroscopic traffic models, see Chapter 10 of [1], fail to explain traffic breakdown i.e. $F \to S$ transition and most of the empirical features of the resulting spatiotemporal congested patterns of traffic flow. This failure is attributed to the fact that these models are in the framework of the fundamental diagram and thus they cannot adequately show the coexistence of free flow, synchronized flow and wide moving jams, whereby the steady states of synchronized flow occupy a 2D region in the flow-density plane. Another factor contributing to these models failure is the absence of the discontinuous character of over-acceleration i.e. the discontinuous character of lane-change probability, as traffic transits from free flow to synchronized flow, which as noted in [1] is one crucial feature of 3-PTT.

Nevertheless, Helbing and co-workers in [28] show the capability of models developed within the framework of fundamental diagram to reproduce many of the empirically observed spatiotemporal congested patterns. Therein, they use the gas-kinetic-based traffic model [4, 37], that has five parameters characterizing the driver-vehicle units. Using two different set of parameters, they show that the model is able to reproduce the congested traffic patterns as shown in their version of the phase diagram. This model, see [4, 37], considers the velocity variance via a velocity variance prefactor that reflects the statistical properties of measured traffic data. Also it is non-local, in that the drivers look-ahead behavior is incorporated. However, looking at the model structure it has a faster-than-traffic wave propagation speed and this is not so desirable as pointed out by Daganzo in [9].

3 Derivation of Macroscopic 3-Phase Traffic Flow Models

3.1 Derivation from the Microscopic Speed Adaptation 3-Phase Traffic Model

The first motivation of this section is the discussion done by Kerner in [1] that existing macroscopic models, which are in the framework of fundamental diagram, fails to adequately reproduce traffic breakdown and the resulting spatial-temporal congested patterns. The second motivation is the work in [2] where the Aw-Rascle model was derived from a microscopic follow-the-leader model and rigorously showed to be the hydrodynamic limit of the time discretization of the microscopic model as the number of vehicles increase, whilst scaling of space and time. We derive a macroscopic traffic flow model coherent with the 3-Phase Traffic Theory (3-PTT) by considering the microscopic Speed Adaptation 3-phase traffic flow model developed in [3], which can be classified as a General Motors (GM) type car-following model. We review the GM type car-following model as follows: Let $x_i(t),\ v_i(t);\ i = 1, ..., N$ be the location and velocity of vehicles at time $t \in \mathbb{R}^+$, and also suppose that the distance headway between two successive vehicles is given by;

$$l_i = x_{i+1} - x_i$$

then we can write the microscopic model equations as follows, compare [2]:

$$\frac{dx_i}{dt} = v_i \tag{3.1}$$

$$\frac{dv_i}{dt} = \frac{C(v_{i+1} - v_i)}{l_i - H} + \frac{U(\rho_i) - v_i}{T} \tag{3.2}$$

where ρ_i is the local "density around vehicle i" which together with its inverse τ_i i.e. the local "specific volume" are expressed in terms of the vehicle length H as follows;

$$\rho_i = \frac{H}{l_i} \qquad and \qquad \tau_i = \frac{1}{\rho_i} = \frac{l_i}{H}. \tag{3.3}$$

$U(\rho_i)$ is a density-dependent optimal velocity. The constant $C > 0$ and the relaxation time T are given parameters.

Remark 3.1.1. *Here the density is normalized and therefore dimensionless so that the maximal density is* $\rho_{jam} = \dfrac{1}{\tau_{jam}} = 1$

The second term on the right of equation (3.2), referred to as the relaxation term, describes the tendency of drivers to accelerate to the density-dependent optimal velocity $U(\rho_i)$ while the first term on the right of equation (3.2) accounts for the dependence of vehicle i acceleration at time t on the relative velocities of this vehicle i and vehicle $i+1$ ahead of it at a clearance $l_i - H$ from vehicle i. Thus the name car-following models. Using τ_i we rewrite the microscopic model (3.1)-(3.2) as;

$$\begin{aligned} \frac{dx_i}{dt} &= v_i \\ \frac{dv_i}{dt} &= \frac{C(v_{i+1} - v_i)}{H(\tau_i - 1)} + \frac{U(\frac{1}{\tau_i}) - v_i}{T} \end{aligned} \tag{3.4}$$

such that

$$\frac{dl_i}{dt} = v_{i+1} - v_i \qquad \Rightarrow \qquad \frac{d\tau_i}{dt} = \frac{v_{i+1} - v_i}{H} \tag{3.5}$$

And defining $a(\rho_i)$ i.e. the speed adaptation coefficient as

$$a(\rho_i) = C\left(\tau_i - 1\right)^{-1} = C\left(\frac{1}{\rho_i} - 1\right)^{-1}. \tag{3.6}$$

We now introduce the microscopic Speed Adaptation model for 3-phase traffic flow as below, compare [3]:

$$\begin{aligned} \frac{dx_i}{dt} &= v_i \\ \frac{dv_i}{dt} &= \frac{a(\rho_i)}{H}\triangle v_i + \begin{cases} \frac{1}{T}(U^{free}(\tau_i) - v_i), & v_i > U_{syn}, \tau_i > \tau_{jam}, \\ \frac{1}{T}(U^{syn}_{av}(\tau_i) - v_i), & v_i < U_{syn}, \tau_i > \tau_{jam}, \\ -\frac{1}{T}v_i, & \tau_i < \tau_{jam}. \end{cases} \end{aligned} \tag{3.7}$$

Remark 3.1.2. *If we choose to use the distance headway* l_i *instead of clearance* $l_i - H$ *in equation (3.2), then we can obtain the 'pressure law'* $p(\rho) = V_{ref} ln(\frac{\rho}{\rho_{jam}})$*, that is considered in [16]. To achieve this, the speed adaptation term in (3.2) can be written as;*

$$\frac{\beta_i(v_{i+1} - v_i)}{l_i} \qquad \Rightarrow \qquad \frac{\beta_i(v_{i+1} - v_i)}{H\tau_i}$$

where now β_i *is the speed adaptation coefficient specified as below;*

$$\beta_i = \beta_i(\rho) = \rho_i V_{ref}$$

with the reference velocity $V_{ref} > 0$ *being a constant.*

A striking difference between the microscopic model of the GM type, equations (3.1)-(3.2) and the above stated microscopic Speed Adaptation model for 3-phase traffic flow, equation (3.7), is in how the relaxation term is prescribed.

Regarding the relaxation term, the model (3.1)-(3.2) is in the framework of the fundamental diagram. From the 3-PTT hypothesis point of view, it means that there is an averaging of the infinite number of steady states of synchronized flow to one synchronized flow velocity for each density in the velocity–density plane. The consequences are that the model will fail to show the very essential features of synchronized flow and also the features of coexistence of free flow, synchronized flow and wide moving jams. In the microscopic Speed Adaptation model (3.7), the 2D region of steady states of synchronized flow is also replaced by a 1D region i.e. by a curve S, given by $U_{av}^{syn}(1/\rho_i)$, in the $\rho u - \rho$ plane and in the associated $\tau - u$ plane as shown in figure 3.1. However, its relaxation term incorporates the $F \to S \to J$ phase transitions of 3-PTT as follows:

- the traffic breakdown i.e. $F \to S$ transition is simulated by a discontinuity between the free flow (F) and the synchronized flow (S) states such that the point of discontinuity in the curve F, given by $U^{free}(1/\rho_i)$, in figure 3.1(a), marks the limit point $((\rho u)_{max}^{free}, \rho_{max}^{free})$ of free flow existence i.e. if $\rho \geq \rho_{max}^{free}$ an $F \to S$ transition will occur.
- the $S \to J$ transition is simulated by supposing that an instability of synchronized flow states exists for densities, $\rho > \rho_{cr}^{(SJ)}$, the critical density for an $S \to J$ transition to occur. For a comprehensive discussion of the microscopic Speed Adaptation model and its variants, see [3].

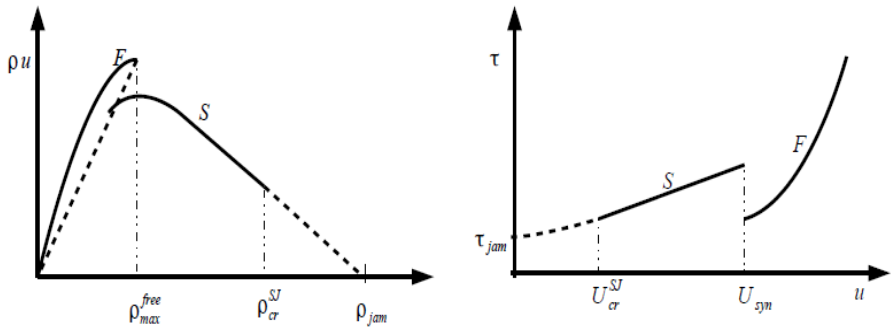

(a) (b)

Figure 3.1: Averaging of the 2D-region steady states of synchronized flow in the microscopic Speed Adaptation model.

A macroscopic description of traffic flow is obviously valid if we consider a large number of vehicles on a sufficiently long stretch of road. Therefore in the limit that

the number of vehicles goes to infinity we can obtain the Lagrangian form of the macroscopic model equations. To this end, we introduce the Lagrangian "mass" coordinates (X, T) whereby $T = t$ and

$$X = \int^{x} \rho(y,t)dy$$

that is not a mass, but rather describes the total length occupied by vehicles up to point x since ρ, in this case, is dimensionless. Now approximating $(v_{i+1} - v_i)/H$ by $\partial_X u$ yields from (3.5) and (3.7) the following Lagrangian form of the macroscopic equations in terms of the following variables: u which is the macroscopic velocity, the (normalized) density ρ that is now the dimensionless fraction of space occupied by vehicles, and its inverse $\tau = \frac{1}{\rho}$ i.e. the specific volume:

$$\begin{aligned} \partial_T \tau - \partial_X u &= 0 \qquad (3.8) \\ \partial_T u - a(1/\tau)\partial_X u &= R(u,\tau) \qquad (3.9) \end{aligned}$$

where

$$R(u,\tau) = \begin{cases} \frac{1}{T}(U^{free}(\tau) - u), & v > U_{syn}, \tau > \tau_{jam}, \\ \frac{1}{T}(U^{syn}_{av}(\tau) - u), & v < U_{syn}, \tau > \tau_{jam}, \\ -\frac{1}{T}u, & \tau < \tau_{jam}. \end{cases} \qquad (3.10)$$

and

$$a(1/\tau) = a(\rho) = C\left(\frac{1}{\rho} - 1\right)^{-1}.$$

To obtain the macroscopic equations in Eulerian coordinates, we change the Lagrangian "mass" coordinates (X, T) into Eulerian coordinates (x, t) with either

$$\partial_x X = \rho, \quad \partial_t X = -\rho u, \quad T = t$$

or

$$\partial_X x = \rho^{-1} = \tau, \quad \partial_T x = u, \quad \partial_X t = 0, \quad \partial_T t = 1.$$

Considering that $x = x(X, T)$ and $t = T$ we have, from (3.8)

$$\partial_t \tau \left(\frac{\partial t}{\partial T}\right) + \partial_x \tau \left(\frac{\partial x}{\partial T}\right) - \partial_x u \left(\frac{\partial x}{\partial X}\right) - \partial_t u \left(\frac{\partial t}{\partial X}\right) = 0.$$

Evaluating the derivatives in the brackets using the above stated relations we get;

$$\partial_t \tau + u\partial_x \tau - \tau \partial_x u = 0 \qquad (3.11)$$

and since $\tau = \frac{1}{\rho}$, (3.11) becomes;

$$-\frac{1}{\rho^2}\partial_t\rho - \frac{1}{\rho^2}u\partial_x\rho - \frac{1}{\rho}\partial_x u = 0$$

which on multiplying through by $-\rho^2$ yields the continuity equation;

$$\partial_t\rho + u\partial_x\rho + \rho\partial_x u = 0. \tag{3.12}$$

From (3.9) we write;

$$\partial_t u\left(\frac{\partial t}{\partial T}\right) + \partial_x u\left(\frac{\partial x}{\partial T}\right) - a(\rho)\left[\partial_t u\left(\frac{\partial t}{\partial X}\right) - \partial_x u\left(\frac{\partial x}{\partial X}\right)\right] = R(u,\tau)$$

and again using the above stated relations we get;

$$\partial_t u + u\partial_x u - a(\rho)\left(\frac{1}{\rho}\right)\partial_x u = R(u,\tau) \tag{3.13}$$

Multiplying (3.13) through by ρ and introducing (3.12) into it, we get;

$$\rho\partial_t u + \rho u\partial_x u + u\left[\partial_t\rho + \partial_x(\rho u)\right] - a(\rho)\partial_x u = \rho R(u,\tau)$$

That is;

$$\left[\rho\partial_t u + u\partial_t\rho\right] + \left[2\rho u\partial_x u + u^2\partial_x\rho\right] - a(\rho)\partial_x u = \rho R(u,\tau)$$

which together with (3.12) yields the following macroscopic Speed Adaptation 3-phase traffic flow model equations of the Aw-Rascle type:

$$\begin{aligned} \partial_t\rho + \partial_x(\rho u) &= 0 \\ \partial_t(\rho u) + \partial_x(\rho u^2) - a(\rho)\partial_x u &= \rho R(u,\tau) \end{aligned} \tag{3.14}$$

Remark 3.1.3. *From the type of the car-following model considered in Remark 3.1.2 one can obtain, by using the above procedures, the following macroscopic Aw-Rascle type traffic model;*

$$\begin{aligned} \partial_t\rho + \partial_x(\rho u) &= 0 \\ \partial_t(\rho u) + \partial_x(\rho u^2) - \rho\beta(\rho)\partial_x u &= \rho R(u,\tau) \end{aligned}$$

whereby $\beta(\rho) = \rho V_{ref}$. This is the model studied in [16] but without the relaxation term $R(.)$.

3.1.1 On the Relaxation Term $R(u, \tau)$

The fundamental hypothesis of the 3-phase traffic theory (3-PTT) is constituted in the microscopic Speed Adaptation model through the relaxation term on the r.h.s. of (3.7). Consequently in the above derived macroscopic Speed Adaptation model (3.14) the 3-PTT hypothesis is taken into account through $R(u, \tau)$, that is presented in (3.10). The 3-PTT hypothesis postulates that the hypothetical steady states of synchronized flow cover a 2D region in the flow-density plane as shown in figure 2.1. However, since the purpose for the development of the microscopic Speed Adaptation model was to simulate the nature of phase transitions in 3-PTT in a simple manner [3], the infinite number of steady states of synchronized flow are averaged such that they now cover a 1D region in the flow-density plane as shown in figure 3.1. In this figure, they are represented by the curve $U_{av}^{syn}(\tau)$, where $\tau = \frac{1}{\rho}$ is viewed here as the space-gap; same as in [3]. The relaxation term (3.10) is such that vehicles decelerate if τ is less than τ_{jam}. We define τ_{jam} as the maximum space gap between vehicles within which the state of traffic can be said to be in the wide moving jam phase. However, if $\tau > \tau_{jam}$ but the vehicles velocity u is less than the parameter U_{syn}, that is the averaged speed within which the steady states of synchronized flow emerges, then the drivers will tend to synchronize their velocities i.e. conform their velocities, to the velocity given by the function $U_{av}^{syn}(\tau)$. Hence the state of traffic is said to be in the synchronized flow phase. Moreover, if $\tau > \tau_{jam}$ but $u > U_{syn}$ then the state of traffic is said to be in free flow phase whereby the drivers accelerate from lower velocities to the optimal speed $U^{free}(\tau)$.

The relaxation term $R(u, \tau)$ can be expressed in an equivalent form $R(u, \rho)$ with the introduction of the mean parameters ρ_{min}^{syn} and ρ_{max}^{free} which are respectively: the minimum density below which synchronized flow cannot occur and the limit density for free flow existence. That is

$$R(u, \rho) \quad = \quad \frac{1}{T}(U^e(\rho, u) - u) \tag{3.15}$$

with,

$$U^e(\rho, u) = \begin{cases} u_1^e(\rho), & \rho < \rho_{min}^{syn}, \quad or \quad u > u_2^e(\rho), u > u_1^e(\rho), \rho < \rho_{max}^{free}, \\ & or \quad u > U_{syn}, \rho_{min}^{syn} < \rho < \rho_{max}^{free}, \\ u_2^e(\rho), & u < U_{syn}, \rho_{min}^{syn} < \rho < \rho_{max}^{free}, \\ & or \quad u < u_2^e(\rho), \rho_{min}^{syn} < \rho < \rho_{max}^{free}, \quad or \quad \rho > \rho_{max}^{free} \end{cases} \tag{3.16}$$

whereby in order to preserve the possibility of the description of very essential features of synchronized flow found in empirical observations, see [1], we opt not to replace the 2D region of steady states of the synchronized flow by a 1D region i.e. by a curve in the flow-density plane. But rather to introduce two density-dependent

optimal velocity curves $u_1^e(\rho)$ and $u_2^e(\rho)$;

$$u_1^e(\rho) = V_o tanh\left[\frac{C_u(1/\rho - h_o)}{c_o V_o}\right]$$
$$u_2^e(\rho) = V_s tanh\left[\frac{C_u(1/\rho - h_s)}{c_s V_s}\right]$$

which are monotone decreasing and satisfy the following properties:

(i) $u_2^e(\rho) = u_1^e(\rho)$, for $\rho < \rho_{min}^{syn}$

(ii) $u_1^e(\rho) > U_{syn} > u_2^e(\rho)$, for $\rho_{min}^{syn} \leq \rho \leq \rho_{max}^{free}$

(iii) $u_1^e(\rho) = u_2^e(\rho)$, for $\rho_{max}^{free} < \rho \leq \rho_{jam}$; $u_1^e(\rho_{jam}) = u_2^e(\rho_{jam}) = 0$

Property (i) is due to the agreement that free flow states can be well represented in the flow-density plane by a curve of positive slope. Thus for densities $\rho < \rho_{min}^{syn}$, vehicles will adjust their velocities u to the optimal velocity $u_1^e(\rho)$. Property (ii) is the critical element of our hypothesis on how the relaxation term constitutes the 3-phase traffic theory. We postulate that for traffic densities within the range $[\rho_{min}^{syn}, \rho_{max}^{free}]$, vehicles will move at different velocities i.e. u will be multivalued. To this aim, we presume that if vehicle velocities $u \leq U_{syn}$ then the drivers will prefer to adjust their velocities to $u_2^e(\rho)$ since the possibilities of overtaking slower vehicles are very low. But if $u > U_{syn}$ the vehicles possibilities of overtaking slower vehicles are higher and therefore there will be the tendency of the drivers to adjust their velocities u to $u_1^e(\rho)$. Property (iii) indicates the situation where the densities are high enough i.e. $\rho > \rho_{max}^{free}$ such that free flow can no longer exist and so the congested state of traffic dominates the flow. This is likely to happen at some location upstream of a road bottleneck after congestion has already set in and the resulting spatialtemporal patterns have propagated upstream. Thereby compeling vehicles velocities to tend to $u_2^e(\rho)$. We note that a continued increase of the density in this traffic state will lead to a complete stop of traffic hence $u_1^e(\rho_{jam}) = u_2^e(\rho_{jam}) = 0$. The above traffic dynamics are illustrated in figure 3.2 whereby the vehicles velocity preferences are portrayed by the direction of the arrows and the length of these arrows denotes the values of $U^e(\rho, u) - u$. The parameters used are presented in table 3.1.

3.2 Derivation from Kinetic Traffic Flow Models

Kinetic traffic flow models are based on a description of the traffic dynamics by distribution functions of velocity of vehicles in traffic flow. Letting this distribution function be denoted by $f(x, v, t)$, it can be interpreted as: at time instant t the expected number of vehicles driving in a road segment $[x, x + dx]$ with velocity in range $[v, v + dv]$ is equal to $f(x, v, t)dxdv$. We consider two kinds of kinetic models for vehicular traffic flows, i.e. kinetic models based on integro-differential equations and those based on the Fokker-Planck type of equations.

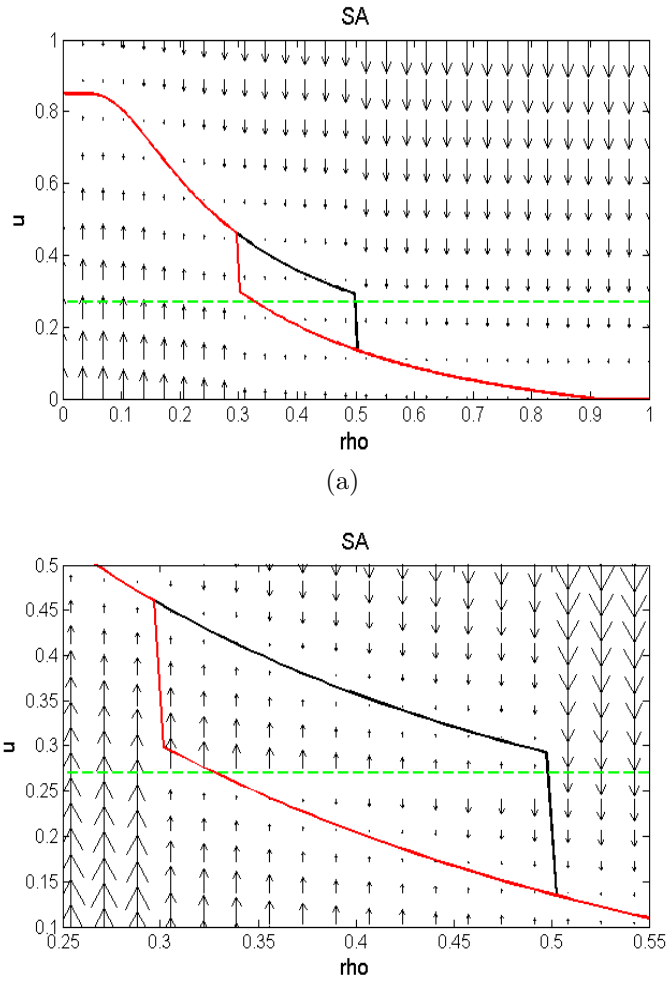

(a)

(b)

Figure 3.2: $U^e(\rho, u) - u$ for the macroscopic Speed Adaptation model. Shown in (b), is a zoom of the 2D region of (a).

3.2.1 Models based on Integro–Differential Equations

There are a number of ways of deriving macroscopic models from the underlying integro-differential equations of kinetic models. It depends on how the pair distribution is decomposed, for example by vehicular chaos assumption, and on the kind of closure relation used to approximate the distribution function. Here we only focus on the procedures used to develop the gas-kinetic-based macroscopic model [4, 5, 7] and the Aw-Rascle type model [6]. In the kinetic models used to develop the above stated macroscopic models, a significant role is played by the pair distribution function $f(x, v, x+h, \hat{v}, t)$ in describing the interaction rates between vehicles at location x driving with velocity v and the leading vehicles at location $x + h$ driving with ve-

locity $\hat{v}$. $h > 0$ being the distance headway between the two considered locations of vehicles. The explicit form of this pair distribution of interacting vehicles yields different kinetic traffic flow models. Now, based on the conservation law, the equation governing the dynamics of distribution function $f = f(x, v, t)$ can, in the case of the model in [7], be given by;

$$\partial_t f + \partial_x(vf) + \partial_v\left(\frac{U_0 - v}{T} f\right) \;=\; (\partial_t f)_{int.} \tag{3.17}$$

upon neglecting lane-change interaction rates; while in [6] it is given by;

$$\partial_t f + \partial_x(vf) \;=\; C^+(f) \tag{3.18}$$

On the l.h.s. of (3.17), the third term describes the tendency of drivers to accelerate to their desired velocities U_0 with a relaxation time T. The r.h.s. term of this equation represents the braking interactions between vehicles, assuming that the braking vehicles decelerate to the exact velocity of the vehicle ahead. It is expressed as follows:

$$(\partial_t f)_{int.} \;=\; \chi P_B\left[G(f) - L(f)\right],$$

where P_B denotes the probability of braking in the situation where a faster vehicle upon encountering a slower vehicle, which it is unable to overtake by changing lanes to a faster lane. χ denotes the effective cross section that accounts for the increased number of vehicle interactions in dense traffic due to vehicular space requirements. And $G(f)$ denotes the gain of $f(x, v, t)$ due to braking of vehicles, while $L(f)$ stands for the loss of $f(x, v, t)$ due to the braking of the vehicles. These functions are given as; see [7]

$$G(f) \;=\; \int_{\hat{v}>v} |v - \hat{v}| f(x, \hat{v}, x + h, v, t) d\hat{v}$$

$$L(f) \;=\; \int_{v>\hat{v}} |v - \hat{v}| f(x, v, x + h, \hat{v}, t) d\hat{v}.$$

In (3.18), the r.h.s. term, that accounts for vehicular interactions due to both acceleration and braking, is given below as in [6]

$$C^+(f) \;=\; \left[G_B^+(f) - L_B^+(f)\right] + \left[G_A^+(f) - L_A^+(f)\right]$$

where the gain and loss terms $G_X^+(f),\ L_X^+(f),\ X = A, B$ due to braking i.e. $X = B$, and due to acceleration i.e. $X = A$ are expressed as in [6] as follows;

$$\begin{aligned} G_B^+(f) = \iint_{\hat{v}>\hat{v}_+} &|\hat{v} - \hat{v}_+| P_B(\hat{v}; .)\sigma_B(v, \hat{v}) \\ &\times f(x, \hat{v}, x + h_B, \hat{v}_+, t) d\hat{v} d\hat{v}_+ \end{aligned} \tag{3.19}$$

Here $\sigma_B(v,\hat{v})$ accounts for the imperfect adaptation of the faster vehicle with velocity $\hat{v}$ to the velocity $\hat{v}_+$ of the slower vehicle ahead during interaction. It is expressed as a probability distribution,

$$\sigma_B(v,\hat{v}) = \frac{\chi_{[\beta\hat{v},\hat{v}]}(v)}{\hat{v}(1-\beta)}, \qquad 0 \leq \beta < 1 \tag{3.20}$$

and indicates how the new velocity v is distributed.

$$L_B^+(f) \;=\; \int_{\hat{v}_+<v} |v-\hat{v}_+| P_B(v;.) f(x,v,x+h_B,\hat{v}_+,t) d\hat{v}_+ \tag{3.21}$$

$$G_A^+(f) \;=\; \iint_{\hat{v}<\hat{v}_+} |\hat{v}-\hat{v}_+| \sigma_A(v,\hat{v}) f(x,\hat{v},x+h_A,\hat{v}_+,t) d\hat{v} d\hat{v}_+ \tag{3.22}$$

where $\sigma_A(v,\hat{v})$ describes the probability with which the slower following vehicles accelerate to a velocity v from $\hat{v}$ after interaction with a faster vehicle ahead, that is moving with velocity $\hat{v}_+ \geq v$. Here,

$$\sigma_A(v,\hat{v}) = \frac{\chi_{[\hat{v},min(V_{max},\alpha\hat{v})]}(v)}{min(V_{max},\alpha\hat{v}) - \hat{v}}, \qquad 1 < \alpha < +\infty \tag{3.23}$$

which indicates how the new velocity is distributed.

$$L_A^+(f) \;=\; \int_{\hat{v}_+>v} |v-\hat{v}_+| f(x,v,x+h_A,\hat{v}_+,t) d\hat{v}_+ \tag{3.24}$$

To evaluate the above integrals, the pair distribution needs to be specified. In [7] it is approximated by a general bivariate Gaussian distribution function as follows;

$$f(x,v,x+h,\hat{v},t) = \rho(x,t)\rho(x+h,t)\frac{\sqrt{det\phi}}{2\pi} exp(-0.5\phi(v,\hat{v})). \tag{3.25}$$

$\phi(v,\hat{v})$ is a positive definite quadratic form that enables the developed model to incorporate the possible correlations between velocities of interacting vehicles (see [7] for its explicit form). $det\phi$ is its determinant and $\rho(.,t)$ is the macroscopic traffic density. In [6] the pair distribution is approximated by a chaos assumption i.e. in terms of the one-vehicle distribution function $f(x,v,t)$ and a leading vehicle distribution function $q(h,v;f)$ as follows;

$$f(x,v,x+h,\hat{v},t) = q(h,v;f) f(x,v,t) F(x+h,\hat{v},t). \tag{3.26}$$

$F(x+h,\hat{v},t)$ denotes the probability distribution in $\hat{v}$ of vehicles at location $x+h$ i.e. $f(x+h,\hat{v},t) = \rho(x+h,t)F(x+h,\hat{v},t)$. The function $q(h;v,f)$ is the distribution

of leading vehicles at a distance h from the considered vehicle with velocity v and assuming that the vehicle velocities are distributed according to $f(x, v, t)$. It is prescribed a priori and should have the following two properties:

$$\int_0^\infty q(h; v, f)dh = 1,$$

and

$$\langle \int_0^\infty hq(h; v, f)dh \rangle = \frac{1}{\rho(x, t)}, \tag{3.27}$$

which implies that the average space gap of the vehicles is $\frac{1}{\rho(x,t)}$.

In derivation of the macroscopic equations from the kinetic equation, the intrinsic macroscopic variables of interest are defined as moments of the distribution function $f(x, v, t)$ as follows;

$$density: \qquad \rho = \rho(x, t) = \int_0^{V_{max}} f(x, v, t)dv$$

$$average\ velocity: \qquad u = u(x, t) = (\rho(x, t))^{-1} \int_0^{V_{max}} vf(x, v, t)dv$$

However, the obtained macroscopic equations are of an infinite hierarchy, in that the macroscopic density equation(i.e. the continuity equation) depends on the average velocity and the macroscopic equation for the average velocity in turn depends on the velocity variance which is given by

$$\theta = \theta(x, t) = (\rho(x, t))^{-1} \int_0^{V_{max}} (v - u)^2 f(x, v, t)dv$$

Since the macroscopic equations for density and velocity dynamics are sufficient to describe the flow of traffic, the hierarchy of equations is closed by assuming that the variance θ is a function of the first two moments i.e. the density and average velocity; and/or by associating the one-vehicle distribution function $f(x, v, t)$ with some probability distribution. In [7], the closure was done by approximating the velocity variance, which is extensively used in the macroscopic version of the vehicle interaction terms therein:

$$\theta = \alpha(\rho)u^2$$

i.e. it is a proportion of the squared average velocity with the density-dependent proportion given by the Fermi function. This closure relation together with the approximation of the pair distribution (3.25) yields the gas-kinetic-based traffic model.

Following the criticism of Daganzo of second-order traffic flow models (i.e.Payne-type models) in [9], Aw and Rascle in [8] revamped research of the second-order traffic models by developing a traffic model that satisfies the principle that the vehicle is an anisotropic particle that mostly responds to frontal stimuli.

Remark 3.2.1. *The gas-kinetic-based traffic model is a Payne-type traffic model. Nevertheless, Helbing and co-worker in [13] defends the model basing their arguments on comparison of the Payne model with the Aw-Rascle model and with the microscopic car-following models.*

Motivated by the work of Aw and Rascle [8], Klar and Wegener [6] derived the Aw-Rascle traffic model from the kinetic model (3.18) by using the relation $f(x,v,t) = \rho F(x,v,t)$, and an ansatz for the stationary equilibrium distribution $f^e(\rho,u,v)$ together with the approximation of the pair distribution given by (3.26). In their derivation of the velocity equation, an additional term that is density-dependent only and involves the velocity variance through the "traffic pressure" emerges. The velocity variance in this case was approximated by;

$$\theta \approx \rho^{-1}\int_0^{V_{max}} (v-u^e(\rho))^2 f^e(\rho,v)dv = \rho^{-1}p^e(\rho)$$

where $p^e(\rho)$ is the approximate "traffic pressure" and under the assumption that u is not too far from its equilibrium value $u^e(\rho)$ i.e. $u^e(\rho)$ is substituted for u. However, this additional term influence was numerically shown to be negligible. Thus the resulting macroscopic model is an Aw-Rascle type traffic model.

In this study we derive a macroscopic 3-phase traffic flow model from the kinetic equation (3.18) by approximating the distribution function using the simplest possible one-node quadrature ansatz [10, 11],

$$f(x,v,t) \approx \rho(x,t)\delta(v-u(x,t)) \tag{3.28}$$

where $\delta(.)$ is the Dirac delta function in the sense of distributions. The limitation of this simple approximation is the disregard of fluctuations in the distribution function $f(x,v,t)$, since (3.28) corresponds to the situation whereby all vehicles present at location x and time instant t move at the same average velocity u, see [12]. However, this limitation is overcome by introducing the relaxation term, which in this study is coherent with 3-phase traffic theory. The advantage of using (3.28) is that it readily yields an Aw-Rascle type macroscopic traffic flow model as will be shown shortly. Moreover, this closure relation approximates the "traffic pressure" by zero i.e.

$$\rho\theta = \int_0^{V_{max}} (v-u)^2 f(x,v,t)dv \approx \int_0^{V_{max}} (v-u)^2\delta(v-u)dv = 0$$

3.2.2 Evaluation of $C^+(f)$ using $f \approx \rho\delta_u(v)$

We use the method of moments to obtain macroscopic equations from kinetic equations by multiplying the inhomogeneous equation (3.18) by $v^k,\ k = 0, 1$ and then integrating with respect to v in the range $[0, V_{max}]$ i.e.

$$\begin{aligned} \partial_t \int_0^{V_{max}} v^k f(x,v,t)dv \ &+ \ \partial_x \int_0^{V_{max}} v^{k+1} f(x,v,t)dv \\ &= \int_0^{V_{max}} v^k C^+(f)(x,v,t)dv \end{aligned} \tag{3.29}$$

Remark 3.2.2. *For the chosen closure relation (3.28), the distribution function $f(x,v,t)$ for one-dimensional flows is fully determined by its first two moments $(M_k,\ k = 0, 1)$ according to the relations;*

$$M_k = \int_0^{V_{max}} v^k f(x,v,t)dv = \rho \int_0^{V_{max}} v^k \delta(v-u)dv = \rho u^k$$

The zeroth moment ,$k = 0$, gives the density ρ while the first moment,$k = 1$, yields the flow rate ρu.

Whilst dropping t, for convenience in writing of the variables, we evaluate the r.h.s. of (3.29) using expressions (3.19)-(3.24) as follows;

Gain from Braking Interaction;

$$\begin{aligned} \int_0^{V_{max}} v^k G_B^+(f)dv &= \int_0^{V_{max}} v^k \iint_{\hat{v}>\hat{v}_+} |\hat{v}-\hat{v}_+| P_B(\hat{v};\rho,u)\sigma_B(v,\hat{v}) \\ &\qquad \times f(x,\hat{v},x+h_B,\hat{v}_+)d\hat{v}d\hat{v}_+dv \\ &= \int_0^{V_{max}} v^k \iint_{\hat{v}>\hat{v}_+} |\hat{v}-\hat{v}_+| P_B(\hat{v};\rho,u)\sigma_B(v,\hat{v}) \\ &\qquad \times q(h_B,\hat{v};f) f(x,\hat{v}) F(x+h_B,\hat{v}_+)d\hat{v}d\hat{v}_+dv \end{aligned}$$

setting $f(x,v) = \rho F(x,v)$, as done in [6], implies that $F(x,v) = \delta_u(v)$ from relation (3.28). Thus;

$$\begin{aligned} \int_0^{V_{max}} v^k G_B^+(f)dv \approx \int_0^{V_{max}} v^k \iint_{\hat{v}>\hat{v}_+} &|\hat{v}-\hat{v}_+| P_B(\hat{v};\rho,u)\sigma_B(v,\hat{v}) q(h_B,\hat{v};\rho) \\ &\times \rho\delta_u(\hat{v})\delta_{u_+}(\hat{v}_+)d\hat{v}d\hat{v}_+dv \end{aligned} \tag{3.30}$$

Loss from Braking Interaction;

$$\begin{aligned}\int_0^{V_{max}} v^k L_B^+(f)dv &= \int_0^{V_{max}} v^k \int_{\hat{v}_+<v} |v-\hat{v}_+| P_B(v;\rho,u) \\ &\times f(x,v,x+h_B,\hat{v}_+,t)d\hat{v}_+dv \\ &= \int_0^{V_{max}} v^k \int_{\hat{v}_+<v} |v-\hat{v}_+| P_B(v;\rho,u)q(h_B,v;f) \\ &\times f(x,v)f(x+h_B,\hat{v}_+,t)d\hat{v}_+dv \\ &\approx \int_0^{V_{max}} v^k \int_{\hat{v}_+<v} |v-\hat{v}_+| P_B(v;\rho,u)q(h_B,v;\rho) \\ &\times \rho\delta_u(v)\delta_{u_+}(\hat{v}_+)d\hat{v}_+dv \end{aligned} \tag{3.31}$$

As a consequence of the Dirac delta function the above gain and loss terms due to braking interactions reduces to;

$$\begin{aligned}\int_0^{V_{max}} v^k \left[G_B^+(f) - L_B^+(f)\right] dv &\approx \rho|u-u_+|P_B(\rho,u)q(h_B;\rho) \\ &\times \left[\int_0^{V_{max}} v^k \sigma_B(v,u)dv - u^k\right] \\ &= \rho|u-u_+|P_B(\rho,u)q(h_B;\rho) \\ &\quad \times \left[\frac{1}{u(1-\beta)}\int_0^{V_{max}} v^k \chi_{[\beta u,u]}(v)dv - u^k\right] \\ &= \rho|u-u_+|P_B(\rho,u)q(h_B;\rho) \\ &\times \left[\frac{1}{u(1-\beta)}\int_{\beta u}^{u} v^k dv - u^k\right] \end{aligned} \tag{3.32}$$

with $u_+ = u(x+h_B)$ which allows us to consider the fact that vehicular interactions are forwardly directed. Noting that braking occurs when $u > u_+$ and that;

$$|u-u_+| = \begin{cases} -(u_+-u), & u > u_+, \\ (u_+-u), & u < u_+. \end{cases} \tag{3.33}$$

we obtain the following from (3.32),

$$\begin{aligned}\int_0^{V_{max}} v^k \left[G_B^+(f) - L_B^+(f)\right] dv &\approx -\frac{\rho(u_+-u)P_B(\rho,u)q(h_B;\rho)}{u(1-\beta)} \\ &\times \left[\frac{u^{k+1}-(\beta u)^{k+1}}{k+1} - u^k\right] \end{aligned}$$

which vanishes for $k=0$ but for $k=1$ we obtain,

$$\begin{aligned}\int_0^{V_{max}} v^k \left[G_B^+(f) - L_B^+(f)\right] dv &\approx -\rho(u_+-u)P_B(\rho,u)q(h_B;\rho) \\ &\times \left[\frac{u(1-\beta)}{2}\right],\ u > u_+ \end{aligned} \tag{3.34}$$

Gain from Acceleration Interaction;

$$\begin{aligned}\int_0^{V_{max}} v^k G_A^+(f)dv &= \int_0^{V_{max}} v^k \iint_{\hat{v}<\hat{v}_+} |\hat{v}-\hat{v}_+|\sigma_A(v,\hat{v}) \\ &\times f(x,\hat{v},x+h_A,\hat{v}_+)d\hat{v}d\hat{v}_+dv \\ &= \int_0^{V_{max}} v^k \iint_{\hat{v}<\hat{v}_+} |\hat{v}-\hat{v}_+|\sigma_A(v,\hat{v})q(h_A,\hat{v};f) \\ &\times f(x,\hat{v})F(x+h_A,\hat{v}_+)d\hat{v}d\hat{v}_+dv \\ &\approx \int_0^{V_{max}} v^k \iint_{\hat{v}<\hat{v}_+} |\hat{v}-\hat{v}_+|\sigma_A(v,\hat{v})q(h_A,\hat{v};\rho) \\ &\times \rho\delta_u(\hat{v})\delta_{u_+}(\hat{v}_+)d\hat{v}d\hat{v}_+dv \end{aligned} \tag{3.35}$$

Loss from Acceleration Interaction;

$$\begin{aligned}\int_0^{V_{max}} v^k L_A^+(f)dv &= \int_0^{V_{max}} v^k \int_{\hat{v}_+>v} |v-\hat{v}_+|f(x,v,x+h_A,\hat{v}_+,t)d\hat{v}_+dv \\ &= \int_0^{V_{max}} v^k \int_{\hat{v}_+>v} |v-\hat{v}_+|q(h_A,v;f)f(x,v) \\ &\times f(x+h_A,\hat{v}_+,t)d\hat{v}_+dv \\ &\approx \int_0^{V_{max}} v^k \int_{\hat{v}_+>v} |v-\hat{v}_+|q(h_A,v;\rho)\rho\delta_u(v)\delta_{u_+}(\hat{v}_+)d\hat{v}_+dv \end{aligned} \tag{3.36}$$

As a consequence of the Dirac delta function the above gain and loss terms due to acceleration interactions reduces to;

$$\begin{aligned}\int_0^{V_{max}} v^k \left[G_A^+(f)-L_A^+(f)\right]dv &\approx \rho|u-u_+|q(h_A;\rho)\left[\int_0^{V_{max}} v^k\sigma_A(v,u)dv-u^k\right] \\ &= \rho|u-u_+|q(h_A;\rho) \\ &\times \left[\frac{1}{\tilde{u}-u}\int_0^{V_{max}} v^k\chi_{[u,\tilde{u}]}(v)dv-u^k\right] \\ &= \rho|u-u_+|q(h_A;\rho)\left[\frac{1}{\tilde{u}-u}\int_u^{\tilde{u}} v^k dv-u^k\right] \end{aligned} \tag{3.37}$$

with $\tilde{u}=min(V_{max},\alpha u)$. Noting that acceleration occurs when $u<u_+$ and using (3.33) we obtain,

$$\int_0^{V_{max}} v^k \left[G_A^+(f)-L_A^+(f)\right]dv \approx \rho(u_+-u)q(h_A;\rho)\left[\frac{\tilde{u}^{k+1}-u^{k+1}}{(k+1)(\tilde{u}-u)}-u^k\right]$$

which vanishes for $k=0$ but for $k=1$ with $\tilde{u}=\alpha u$ we obtain,

$$\int_0^{V_{max}} v^k \left[G_A^+(f)-L_A^+(f)\right]dv \approx \rho(u_+-u)q(h_A;\rho)\left[\frac{\alpha u-u}{2}\right], \quad u<u_+ \tag{3.38}$$

Using Taylor approximation $u(x+h)-u(x) \approx h\partial_x u$ on (3.34) and (3.38) we get;

$$\int_0^{V_{max}} v^k C^+(f)dv \approx \begin{cases} \rho h_B P_B(\rho,u) q(h_B;\rho)\dfrac{1-\beta}{2} u\partial_x u, & \partial_x u < 0, \\ \rho h_A q(h_A;\rho)\dfrac{\alpha-1}{2} u\partial_x u, & \partial_x u > 0 \end{cases}. \tag{3.39}$$

We can assume that the leading vehicles are distributed in such a way that;

$$h_B q(h_B;\rho) = h_A q(h_A;\rho) = \frac{db(\rho)}{d\rho} \tag{3.40}$$

where $b(\rho)$ is some increasing function of density ρ, whose exact form will be deduced in a little while. Thus we obtain the following Aw-Rascle type macroscopic equations;

$$\begin{aligned} \partial_t \rho + \partial_x(\rho u) &= 0 \\ \partial_t(\rho u) + \partial_x(\rho u^2) - a(\rho,u)\partial_x u &= 0 \end{aligned} \tag{3.41}$$

where $a(\rho,u)$ is deduced from (3.39) and written as;

$$a(\rho,u) = \begin{cases} \rho\dfrac{db(\rho)}{d\rho}\varphi_B(\rho,u), & \partial_x u < 0, \\ \rho\dfrac{db(\rho)}{d\rho}\varphi_A(u), & \partial_x u > 0 \end{cases}.$$

with suitable functions $\varphi_A(u)$, $\varphi_B(\rho,u)$. We can make further simplifications by approximating $\varphi_A(u)$, $\varphi_B(\rho,u)$ by a constant C to obtain the coefficient,

$$a(\rho) = C\rho\frac{db(\rho)}{d\rho} \tag{3.42}$$

From (3.6) we find that $b(\rho)$ takes the form;

$$b(\rho) = -ln\left[1-\rho\right] \tag{3.43}$$

3.2.3 Models based on Fokker-Planck Equations

We consider the following Fokker-Planck type traffic flow model, i.e. the kinetic traffic flow model developed in [38], but neglecting the diffusion term and the lane-changing rates:

$$\partial_t f + \partial_x(vf) + \partial_v\left(B\left[f\right]f\right) = 0. \tag{3.44}$$

Here $B[f]$ describes vehicle braking/acceleration behaviour in response to traffic situations and can be expressed as in [38]:

$$B[f](x,v,t) = \begin{cases} -c_B\rho^B P_B(u^B,v)|v-u^B|^\eta, & v > u^B, \\ c_A(\rho_{max}-\rho^A)|u^A-v|^\eta, & v \le u^B,\ v \le u^A, \\ 0, & otherwise \end{cases}$$

with $\rho^X = \rho(x+h_X,t)$, $u^X = u(x+h_X,t)$, for $X = A, B$. $P_B(u^B,v)$ represents the probability of braking. $\eta = 1, 2$ and c_A, c_B are dimensionless constants for $\eta = 2$. In the case that $\eta = 1$, we suppose that $c_B\rho^B P_B = Cq(h_B;\rho)$ and $c_A(\rho_{max}-\rho^A) = Cq(h_A;\rho)$, where $q(h_A;\rho), q(h_B;\rho)$ are defined as before and with C as a constant. Hence for $\eta = 1$ we can write the braking/acceleration term as follows:

$$B[f](x,v,t) = \begin{cases} -Cq_B|v-u^B|, & v > u^B, \\ Cq_A|u^A-v|, & v \le u^B,\ v \le u^A, \\ 0, & otherwise \end{cases} \tag{3.45}$$

Now to obtain a macroscopic model from the kinetic model (3.44) with $B[f]$ given as in (3.45), we use the one-node quadrature ansatz (3.28) to approximate the distribution function $f = f(x,v,t)$ in evaluating the integrals in the following expression; for $k = 0, 1$.

$$\partial_t \int_0^{V_{max}} v^k f dv + \partial_x \int_0^{V_{max}} v^{k+1} f dv + \int_0^{V_{max}} v^k \partial_v (B[f] f)\, dv = 0 \tag{3.46}$$

Evaluation of the third term in the l.h.s. of (3.46) can be done by integration by parts as follows:

$$\int_0^{V_{max}} v^k \partial_v (B[f] f)\, dv = \left[v^k B[f] f\right]_0^{V_{max}} - \int_0^{V_{max}} k v^{k-1} B[f] f dv. \tag{3.47}$$

Noting that the velocity distribution function is such that $f(0) = f(V_{max}) = 0$, the l.h.s. of (3.47) vanishes for $k = 0$. But for $k = 1$ we can write;

$$\int_0^{V_{max}} v \partial_v (B[f] f)\, dv = -\int_0^{u^B} B[f] f dv - \int_{u^B}^{V_{max}} B[f] f dv. \tag{3.48}$$

Considering the ansatz $f \approx \delta_u(v)$, if the average velocity $u \le u^B$ the second term on r.h.s. of (3.48) vanishes but the first term becomes:

$$-\int_0^{u^B} B[f] f dv \approx -C\rho q_A|u^A - u| \quad , \quad v \le u^B,\ v \le u^A$$

Else if $u > u^B$ the first term on r.h.s. of (3.48) vanishes but the second term becomes:

$$-\int_{u^B}^{V_{max}} B\left[f\right] f dv \approx C\rho q_B |u - u^B| \quad , \quad v > u^B$$

Altogether, we obtain;

$$\int_0^{V_{max}} v\partial_v \left(B\left[f\right] f\right) dv \approx \begin{cases} C\rho q_B |u - u^B|, & u > u^B, \\ -C\rho q_A |u^A - u|, & u \leq u^B,\ u \leq u^A, \\ 0, & otherwise \end{cases} \tag{3.49}$$

Using the following definitions;

$$|u - u^B| \;=\; \begin{cases} -(u^B - u), & u > u^B, \\ (u^B - u), & u < u^B. \end{cases}$$

$$|u^A - u| \;=\; \begin{cases} (u^A - u), & u^A > u, \\ -(u^A - u), & u^A < u. \end{cases}$$

and the approximation $u^X - u \approx h_X \partial_x u$ for $X = A, B$, expressions (3.48) and (3.49) yields;

$$\int_0^{V_{max}} v\partial_v \left(B\left[f\right] f\right) dv \;\approx\; \begin{cases} -C\rho q_B h_B \partial_x u; & \partial_x u < 0 \\ -C\rho q_A h_A \partial_x u; & \partial_x u > 0 \end{cases} . \tag{3.50}$$

Choosing $h_A q_A$ and $h_B q_B$ as in (3.40) we obtain the coefficient (3.42), i.e.

$$a(\rho) = C\frac{\rho}{1-\rho} \tag{3.51}$$

Therefore, from (3.46) we obtain the Aw-Rascle type macroscopic equations (3.41) with the coefficient a now given as in (3.51). Introducing the relaxation term $R(u, \rho)$ i.e. equation (3.15) to the r.h.s. of equation (3.41) while using coefficient (3.51), that is coefficient (3.42), we obtain the following macroscopic 3-phase traffic flow model from the considered kinetic traffic models:

$$\begin{aligned} \partial_t \rho + \partial_x(\rho u) &= 0 \\ \partial_t(\rho u) + \partial_x(\rho u^2) - a(\rho)\partial_x u &= \rho R(u, \rho) \end{aligned} \tag{3.52}$$

Remark 3.2.3. *If we set $h_A q_A = h_B q_B = \rho$ in both (3.39) and (3.50) and also let $C = V_{ref}$, then the coefficient $a(\rho)$ in (3.42) and (3.51) becomes $a(\rho) = V_{ref}\rho^2$. Thus the l.h.s. of (3.52) becomes the model studied in [16], which has the 'pressure law' $p(\rho) = V_{ref} ln(\frac{\rho}{\rho_{jam}})$.*

In this section we have shown the derivation of macroscopic model equations from the kinetic equations. And as shown in [40], one obtains macroscopic equations regardless of whether one uses a kinetic model based on an integro-differential equation or the Fokker-Planck type equation. In model (3.52) we simply use the relaxation term (3.15) that is deduced from the microscopic Speed Adaptation model (3.7). This kind of relaxation term, unlike the classical ones, yields a multi-valued fundamental diagram. It is shown in [41] that the multi-valued fundamental diagram can be obtained from a kinetic model. This is made possible by use of the braking probability in the relaxation term of the kinetic model. In section 3.3 we determine, explicitly in terms of ρ and u, the macroscopic equivalence of the relaxation term in the kinetic model [41] by applying linear interpolation in the relaxation term of the Switching Curve traffic flow model presented in [14].

3.3 Derivation from the Switching Curve Traffic Flow Model

In the Switching Curve traffic flow model presented in [14], two equilibrium velocity curves $U_1(\rho)$, $U_2(\rho)$ are proposed. This follows from the fact that, for traffic flow on multilane freeways, one often observes distinct stable equilibrium relationships between traffic velocity and density. The two curves are monotone decreasing and are such that $U_2(\rho) < U_1(\rho)$, $0 \leq \rho < \rho_{max}$ with $U_1(\rho_{max}) = U_2(\rho_{max}) = 0$ as shown in figure 3.3(a). These characterize two modes in which the state of traffic occur

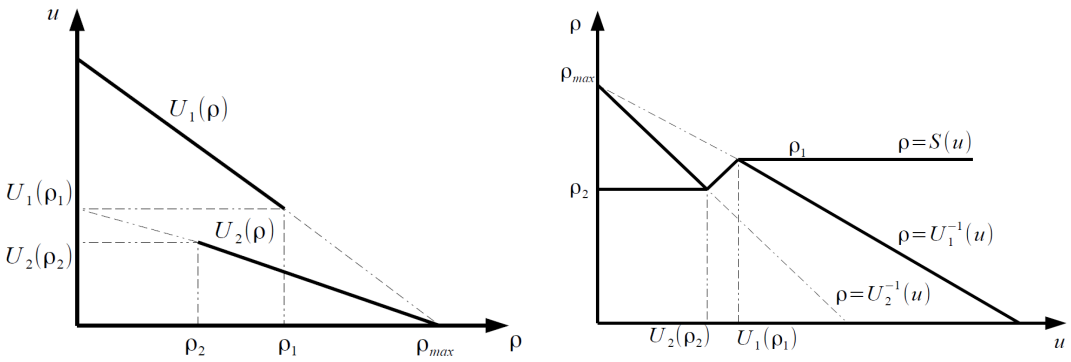

(a) (b)

Figure 3.3: Shown in (a), are the two equilibrium velocity curves $U_1(\rho)$ and $U_2(\rho)$, while (b) shows the switching curve $S(u)$.

i.e. the upper curve $U_1(\rho)$ characterize the fast mode, where the traffic is less dense and thus enabling easy lane change and overtaking maneuvres; and the lower curve

$U_2(\rho)$ characterize the slower mode, where traffic is more dense and thus yielding a significant decline in lane change and overtaking maneuvres. The characteristic feature of this model is the existence of a switch curve, $\rho = S(u)$ for $u \geq 0$, that is a monotone non-decreasing function satisfying the following: see figure 3.3(b).

$$S(u) = \rho_2, \quad 0 \leq u \leq U_2(\rho_2), \qquad and \qquad S(u) = \rho_1, \quad u \geq U_1(\rho_1) \tag{3.53}$$

whereby $0 < \rho_2 \leq \rho_1 < \rho_{max}$ with $U_2(\rho_2) \leq U_1(\rho_1)$. The governing equations of the Switching Curve model can be given as; see [14].

$$\begin{aligned} \partial_t \rho + \partial_x(\rho u) &= 0 \\ \partial_t(\rho u) + \partial_x(\rho u^2) + \rho U_1'(\rho)\partial_x u &= \rho R(u,\rho) \end{aligned} \tag{3.54}$$

with

$$R(u,\rho) = \begin{cases} \frac{1}{T}(U_1(\rho) - u), & \rho < S(u), \\ \frac{1}{T}(U_2(\rho) - u), & \rho \geq S(u), \end{cases}. \tag{3.55}$$

and $U_1'(\rho) = \partial_\rho (U_1(\rho)) \leq 0$. Here we simply let $U_1'(\rho) = -\frac{a(\rho)}{\rho}$. The switching mechanism postulated in (3.55) is as follows: if the current traffic state, (ρ, u), lies below $\rho = S(u)$, drivers preferences will tend towards the fast equilibrium curve $u = U_1(\rho)$, whereas if the traffic state lies above $\rho = S(u)$, the drivers preferences now will tend towards the slow equilibrium curve $u = U_2(\rho)$.

Now setting $\rho_1 = \rho_{max}^{free}$ and $\rho_2 = \rho_{min}^{syn}$ we can write the equivalent of $R(\rho, u)$ in (3.55) as;

$$R(u,\rho) = \frac{1}{T}(U^e(\rho,u) - u) \tag{3.56}$$

with,

$$U^e(\rho,u) = \begin{cases} u_1^e(\rho), & \rho < \rho_{min}^{syn}, \quad or \quad u > R(\rho), \rho_{min}^{syn} < \rho < \rho_{max}^{free}, \\ u_2^e(\rho), & u < R(\rho), \rho_{min}^{syn} < \rho < \rho_{max}^{free}, \quad or \quad \rho > \rho_{max}^{free} \end{cases} \tag{3.57}$$

where now the switching curve is $R(\rho)$; viewing the traffic dynamics from the perspective of density. The optimal velocity curves $u_1^e(\rho)$ and $u_2^e(\rho)$ are the same monotone decreasing functions of density as defined in section 3.1, but satisfying a different property (ii), which is now given by;

$$u_1^e(\rho) > R(\rho) > u_2^e(\rho), \quad \rho_{min}^{syn} < \rho < \rho_{max}^{free}$$

whereby

$$u_2^e(\rho_{min}^{syn}) = R(\rho_{min}^{syn}), \quad u_1^e(\rho_{max}^{free}) = R(\rho_{max}^{free})$$

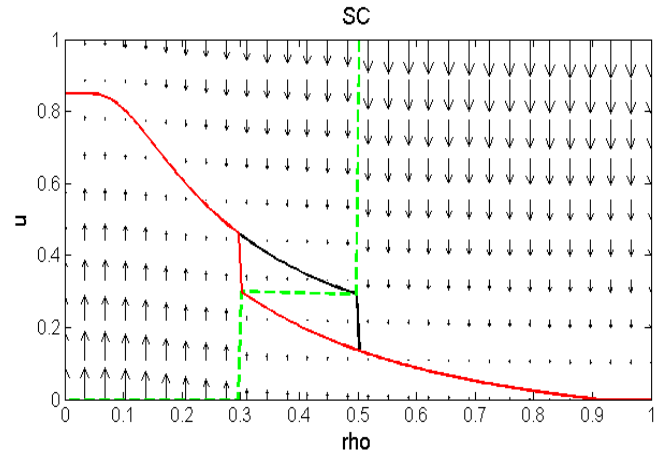

(a)

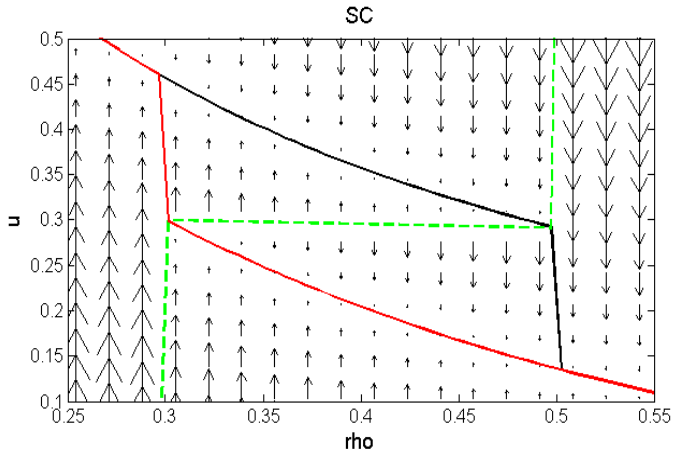

(b)

Figure 3.4: $U^e(\rho, u) - u$ for the Switching Curve model. Shown in (b), is a zoom of the 2D region of (a).

as shown in figure 3.4. The explanations given in section 3.1 for the properties (i) and (iii) also holds for this kind of relaxation term; only that in the explanation given under property (ii), we replace the constant line U_{syn} with the curve $R(\rho)$, that is an increasing function of density for $\rho \in [\rho_{min}^{syn}, \rho_{max}^{free}]$. In figure 3.4 just as in figure 3.2 the vehicles velocity preferences are depicted together with the values of $U^e(\rho, u) - u$. Notice that inside the density range $[\rho_{min}^{syn}, \rho_{max}^{free}]$ and also within the confines of the optimal curves $u_1^e(\rho)$ and $u_2^e(\rho)$, the arrows close to the curve $R(\rho)$ (in figure 3.4) and line U_{syn} (in figure 3.2) have more length than those further away as we tend to the optimal curves. This is not the case in the following modified Switching Curve model, see figure 3.6. The parameters used to generate these figures are given in table 3.1.

Note that the model equations (3.52) yields a 3-phase traffic flow model because the 3-phase traffic theory(3-PTT) hypothesis has been constituted in the model through the relaxation term (3.15). However, in the Switching Curve model (3.54), the manner in which the relaxation term is specified, see (3.56), does not actually yield a 3-phase traffic flow model. Indeed, simulations of (3.52) with the relaxation term (3.56) (presented in Chapter 4) reveals that moving jams emerge spontaneously at the onset of congestion at a road bottleneck, which is contrary to 3-PTT which advocates that traffic congestion is a sequence of first order $F \to S \to J$ transitions. Nevertheless, we can modify the relaxation term (3.56) to obtain a 3-phase traffic flow model by linear interpolation as follows: From the plot of $U^e(\rho, u) - u$ in figure 3.4 at $\rho = \bar{\rho} = 0.4$ we deduce the diagram shown in figure 3.5. There we do the

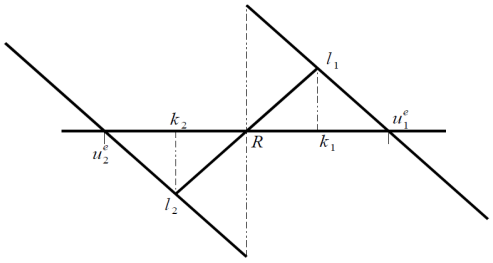

Figure 3.5: Modification of Switching Curve model by linear interpolation.

linear interpolation by introducing parameters k_1,k_2 as below;

$$\begin{aligned} k_1 &= u_1^e(\bar{\rho}) + \alpha(R(\bar{\rho}) - u_1^e(\bar{\rho})) \\ k_2 &= u_2^e(\bar{\rho}) + \alpha(R(\bar{\rho}) - u_2^e(\bar{\rho})) \qquad ; \quad 0 < \alpha < 1 \end{aligned}$$

Since the slope of the lines upon which segments $l_1u_1^e$ and $u_2^el_2$ lie is -1, we have

$$-1 = \frac{0 - l_1}{u_1^e - k_1} \qquad ; \quad k_1 < u_1^e, \quad l_1 > 0$$

$$-1 = \frac{l_2 - 0}{k_2 - u_2^e} \qquad ; \quad k_2 > u_2^e, \quad l_2 < 0$$

which yields $l_1 = u_1^e - k_1$ and $l_2 = u_2^e - k_2$. Next we determine the slope of line segment l_1l_2 that cuts through R at fixed density $\bar{\rho}$ as;

$$s = \frac{l_1 - l_2}{k_1 - k_2} = \frac{(u_1^e - k_1) - (u_2^e - k_2)}{k_1 - k_2}$$

This will certainly be the slope of any line segment l_1l_2 cutting through $R(\bar{\rho})$ for a fixed density $\bar{\rho}$ chosen from the range $\left[\rho_{min}^{syn}, \rho_{max}^{free}\right]$. Since we know that all these

lines should cut through $R(\bar{\rho})$ at which $U^e(\bar{\rho}, u) - u = 0$ we make use of the straight-line equation in its "slope-intercept" form to obtain the intercept c of lines $l_1 l_2$ that passes through point $(R(\bar{\rho}), 0)$ as follows;

$$0 = sR(\bar{\rho}) + c \qquad \Rightarrow \qquad c = -sR(\bar{\rho})$$

Therefore the linear interpolation between surfaces $u_1^e(\rho) - u$ and $u_2^e(\rho) - u$ for $\rho \in \left[\rho_{min}^{syn}, \rho_{max}^{free}\right]$ is described by the equation;

$$u_*(\rho) = s(u - R(\rho)) \quad ; \quad \rho \in \left[\rho_{min}^{syn}, \rho_{max}^{free}\right] \tag{3.58}$$

The above procedure yields the following relaxation term that is capable of reproducing the traffic breakdown phenomenon of 3-PTT.

$$R(u, \rho) \;=\; \frac{1}{T}(U^e(\rho, u) - u) \tag{3.59}$$

with,

$$U^e(\rho, u) = \begin{cases} u_1^e(\rho), & \rho < \rho_{min}^{syn}, \quad or \quad u > u_2^e(\rho), u > u_1^e(\rho), \rho < \rho_{max}^{free}, \\ u_*(\rho) + u, & u_2^e(\rho) < u < u_1^e(\rho), \rho_{min}^{syn} < \rho < \rho_{max}^{free}, \\ u_2^e(\rho), & u < u_2^e(\rho), \rho_{min}^{syn} < \rho < \rho_{max}^{free}, \quad or \quad \rho > \rho_{max}^{free} \end{cases}$$

Hence from the Switching Curve traffic model (3.54) with (3.56) we obtain a macroscopic 3-phase traffic flow model i.e. the modified Switching Curve model given by (3.52) but with the relaxation term defined as in (3.59). In this relaxation term, we still consider the same optimal velocity curves but which are hereby required to satisfy only the previously defined properties (i) and (iii). Now due to the linear interpolation done to modify the Switching Curve model in order to obtain a 3-phase traffic flow model, property (ii) is altered to;

$$u_1^e(\rho) > (u_*(\rho) + u) > u_2^e(\rho), \quad \rho_{min}^{syn} < \rho < \rho_{max}^{free}$$

with

$$u_2^e(\rho_{min}^{syn}) = R(\rho_{min}^{syn}), \quad u_1^e(\rho_{max}^{free}) = R(\rho_{max}^{free})$$

and whereby $u_*(\rho) + u$ is another solution in addition to the equilibrium solutions $u_1^e(\rho)$ and $u_2^e(\rho)$, of the equation;

$$u = U^e(\rho, u) \tag{3.60}$$

for a given ρ within the range $[\rho_{min}^{syn}, \rho_{max}^{free}]$. That is the equation has 3 different solutions which are consistent with the 3-PTT hypothesis, which says that the steady states of synchronized flow should cover a 2D region in the flow-density plane and consequently in the velocity-density plane. This 2D region is the place where the

multivalued solutions to (3.60) are located. From another perspective, while considering (3.60), we write that the value of $U^e(\rho, u) - u$ should vanish at the solutions of (3.60), i.e. the arrows diminish at the solutions, as shown in figure 3.6. Notice the third solution $u_*(\rho) + u$ is located along the curve $R(\rho)$ for some $\rho \in [\rho_{min}^{syn}, \rho_{max}^{free}]$. Now if (3.60) had a unique solution in the density range $[\rho_{min}^{syn}, \rho_{max}^{free}]$ just like it normally does for any $\rho < \rho_{min}^{syn}$ (see figure 3.6) then we would obtain a well defined relation for equilibrium velocity and density, then the usual fundamental diagram would result. That is to mean, the 2D region of synchronized flow would vanish and in place we would have a 1D region i.e. a curve on the velocity-density plane and also on the flow-density plane.

Table 3.1: Relaxation term parameters (dimensionless).

C_u	0.45	V_o	0.85
ρ_{max}^{free}	0.5	h_o	0.05
ρ_{min}^{syn}	0.3	c_o	2.9
ρ_{jam}	0.95	V_s	0.5
U_{syn}	0.28	h_s	1.1
α	0.7	c_s	2.9

3.4 Features of the Derived Macroscopic 3-Phase Traffic Flow Model

The macroscopic traffic flow models derived in the previous sections i.e. the macroscopic Speed Adaptation model (3.14), (3.15) in section 3.1, the Switching Curve model equations (3.54), (3.56) with $U_1'(\rho) = -\frac{a(\rho)}{\rho}$ in section 3.3 and the modified Switching Curve model (3.52), (3.59), only differ in how the relaxation term is prescribed. Otherwise, the l.h.s. of the system of partial differential equations is the same and it is sufficient in showing the main features as far as the models solutions are concerned. Therefore, in this section we discuss the features of the Aw-Rascle type system;

$$\partial_t \rho + \partial_x(\rho u) = 0 \tag{3.61}$$

$$\partial_t(\rho u) + \partial_x(\rho u^2) - a(\rho)\partial_x u = 0 \tag{3.62}$$

Depending on how we recast equation (3.62), we can rewrite the above system in two forms. That is;

Non conservative form: This is in terms of the primitive variables ρ and u.

$$\partial_t \rho + \partial_x(\rho u) = 0 \tag{3.63}$$

$$\partial_t u + (u - \frac{a(\rho)}{\rho})\partial_x u = 0 \tag{3.64}$$

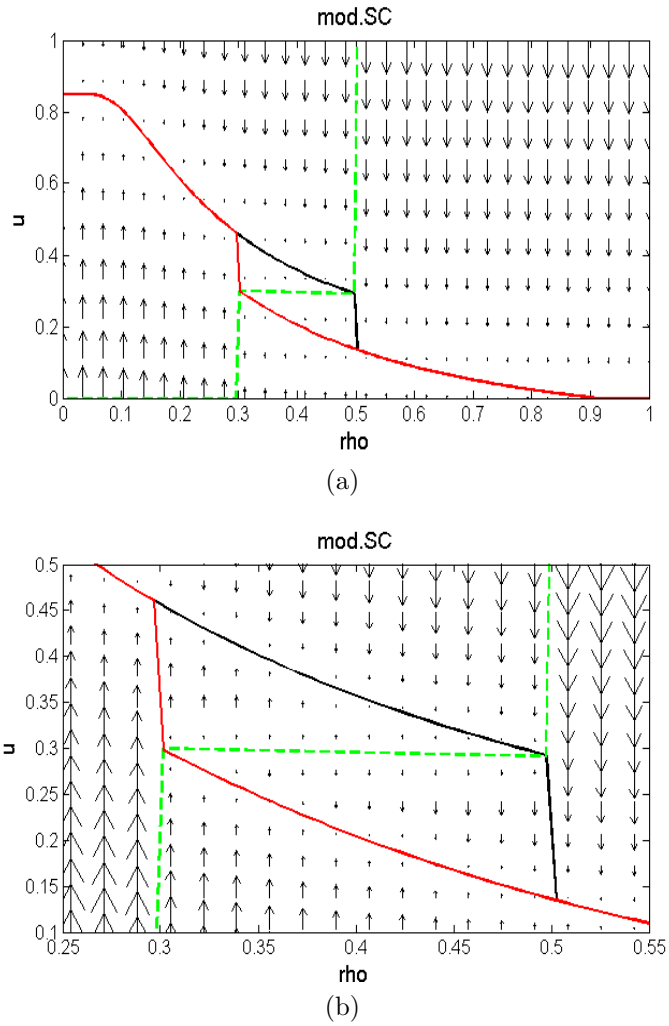

(a)

(b)

Figure 3.6: $U^e(\rho, u) - u$ for the modified Switching Curve model. Shown in (b), is a zoom of the 2D region of (a).

whereby equation (3.64) describes the change of velocity u in space and time. It is obtained by use of the mass conservation equation (3.63) in the flow rate equation (3.64) as;

$$\rho\partial_t u + u\underbrace{\partial_t\rho + u\partial_x\rho + \rho\partial_x u}_{=0} + (\rho u - a(\rho))\partial_x u \quad = \quad 0 \tag{3.65}$$

and upon dividing through by ρ. For clarity, we use the following expression;

$$\frac{a(\rho)}{\rho} = \rho\frac{C}{\rho(1-\rho)} = \rho p\prime(\rho) \tag{3.66}$$

where the prime denotes differentiation with respect to ρ.

Conservative form: Multiplying equation (3.61) by $p\prime(\rho)$ we have;

$$p\prime(\rho)(\partial_t\rho + u\partial_x\rho + \rho\partial_x u) = 0 \quad \Rightarrow \quad \rho p\prime(\rho)\partial_x u = -p\prime(\rho)(\partial_t\rho + u\partial_x\rho)$$

which enables (3.64) to be rewritten as;

$$\partial_t u + u\partial_x u + p\prime(\rho)(\partial_t\rho + u\partial_x\rho) \;=\; 0$$

or,

$$\partial_t(u + p(\rho)) + u\partial_x(u + p(\rho)) \;=\; 0 \tag{3.67}$$

Now multiplying equation (3.61) by the term, $u + p(\rho)$, and equation (3.67) by ρ we add the resulting equations to get;

$$(u + p(\rho))\partial_t\rho + (u + p(\rho))\partial_x(\rho u) + \rho\partial_t(u + p(\rho)) + \rho u\partial_x(u + p(\rho)) = 0$$

which can be rearranged and then combined with (3.61) to yield the following conservative form of the considered system;

$$\partial_t\rho + \partial_x(\rho u) \;=\; 0 \tag{3.68}$$

$$\partial_t[\rho(u + p(\rho))] + \partial_x[\rho u(u + p(\rho))] \;=\; 0 \tag{3.69}$$

where the conservative variables are ρ and

$$y := \rho u + \rho p(\rho)) \tag{3.70}$$

However, unlike in gas dynamics where the second equation of a system in conserved form would have a natural interpretation as the conservation of momentum, (3.69) is not derived from any conservation principle because conservation of momentum does not have a direct physical interpretation in traffic flow. Hence there is no direct physical interpretation of the conservative variable y. It is somewhat heuristic. Note that the system (3.61)-(3.62) and (3.63)-(3.64) are identical for smooth solutions. Therefore, we use the system (3.63)-(3.64) to show the hyperbolic features of the derived macroscopic traffic model by expressing it in a vector form using a vector $V = (\rho, u)^T$ of primitive variables:

$$\partial_t V + A(V)\partial_x V \;=\; 0 \tag{3.71}$$

where,

$$A(V) = \begin{pmatrix} u & \rho \\ 0 & u - \rho p\prime(\rho) \end{pmatrix} \tag{3.72}$$

Now, the properties of the system are largely dictated by the eigenvalues of the Jacobian matrix $A(V)$, that are determined by the characteristic polynomial,

$$det(A - \lambda I) = 0$$

These eigenvalues are the characteristic speeds that govern the propagation of information in the traffic stream. Therefore system (3.63)-(3.64) and consequently the macroscopic traffic flow models are strictly hyperbolic, because calculation of the eigenvalues of $A(V)$ yields the following;

$$\lambda_1(V) = u - \rho p\prime(\rho) < u, \qquad \lambda_2(V) = u \quad ; \quad \rho \neq 0$$

with the largest eigenvalue equal to the traffic flow velocity u. This means that no traffic information travels faster than the traffic and so the anisotropic character of vehicular traffic flow is preserved. In the ensuing we will refer to waves associated with λ_1 as 1-waves and to those associated with λ_2 as 2-waves. In order to determine these waves we determine the right eigenvectors $R^{(i)} = (r_1^{(i)}, r_2^{(i)})$ of the matrix $A(V)$ corresponding to the eigenvalues λ_i from,

$$AR^{(i)} = \lambda_i R^{(i)} \, ; i = 1, 2 \tag{3.73}$$

On solving (3.73) for each eigenvalue we readily obtain,

$$R^1(V) = \begin{pmatrix} 1 \\ \\ -p\prime(\rho) \end{pmatrix} \quad , \qquad R^2(V) = \begin{pmatrix} 1 \\ \\ 0 \end{pmatrix}$$

Letting ∇ be the gradient with respect to $V = (\rho, u)^T$ we determine the kind of waves associated to each eigenvalue $\lambda_i, i = 1, 2$, by checking whether the dot product $\nabla\lambda_i(V) \cdot R^{(i)}(V)$ vanishes or not. Precisely, for $\lambda_1(V) = u - \rho p\prime(\rho)$ we have;

$$\begin{pmatrix} \partial_\rho \lambda_1 \\ \\ \partial_u \lambda_1 \end{pmatrix} \cdot \begin{pmatrix} 1 \\ \\ -p\prime(\rho) \end{pmatrix} = -\partial_\rho(\rho p\prime(\rho)) - p\prime(\rho) \neq 0$$

implying that 1^{st} characterisitc field is genuinely nonlinear. For $\lambda_2(V) = u$ we have;

$$\begin{pmatrix} \partial_\rho \lambda_2 \\ \\ \partial_u \lambda_2 \end{pmatrix} \cdot \begin{pmatrix} 1 \\ \\ 0 \end{pmatrix} = 0$$

that is the 2^{nd} characterisitc field is linearly degenerate. As a result of the above, the 1-waves will be either a rarefaction or shock wave and the 2-waves will be contact discontinuities. Note that a shock is a jump discontinuity associated with the 1^{st} characteristic and a contact discontinuity is also a jump discontinuity associated with the 2^{nd} characteristic . The 1-and 2-waves aid in solving the Riemann problem. The jump discontinuities have to be regarded in the conservative form (3.68)-(3.69). We now discuss the construction of solutions to the Riemann problem.

3.4.1 The Riemann Problem and its Solution

Using the conservative form (3.68)-(3.69) of the Aw-Rascle type traffic model we set up the Riemann problem with piecewise constant initial data as follows;

$$\begin{cases} \partial_t U + \partial_x F(U) = 0 \\ U(x,0) = \begin{cases} U_L & if \quad x < 0 \\ U_R & if \quad x > 0 \end{cases} \end{cases} \tag{3.74}$$

where $U = (\rho, y)^T$, $F(U) = (\rho u, yu)^T$ and $U_L(U_R)$ is the piecewise constant traffic state on the left(right) of the jump located at $x = 0$. Since $\lambda_1(\rho, u) < \lambda_2(\rho, u)$, for all U, then 1-waves must precede 2-waves, see [15]. Thus the general solution of the Riemann problem includes: a 1-wave connecting the left state U_L to an intermediate state U_M (to be defined) and a 2-wave connecting this intermediate state U_M to the right state U_R. Now because the 1-waves can either be shocks or rarefaction waves, there will be the following types of solutions,

- 1-shock connecting U_L to U_M followed by a 2-contact discontinuity connecting U_M to U_R. Note here that the shock speed S_1 can be less than zero or greater than zero as in figures 3.7(a),(b) respectively.
- 1-rarefaction wave connecting U_L to U_M followed by a 2-contact discontinuity connecting U_M to U_R. The right edge of the fan is denoted by S_H (i.e. the rarefaction head) and the left edge of the fan is denoted by S_T (i.e. the rarefaction tail). See figure 3.8. Note that in the case of a 1-shock, $S_T = S_H = S_1$

Of course $U_M = U_R(U_M = U_L)$, if $U_L$and U_R are connected by only a 1-wave(2-wave). To determine the intermediate state U_M we need to compute the Riemann

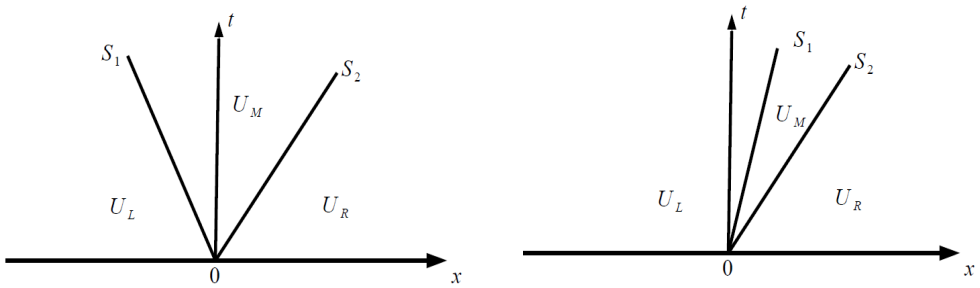

(a) (b)

Figure 3.7: Possible shock solutions to the Riemann problem.

invariants in the sense of Lax and use the i-Lax curves (associated to the i-waves,

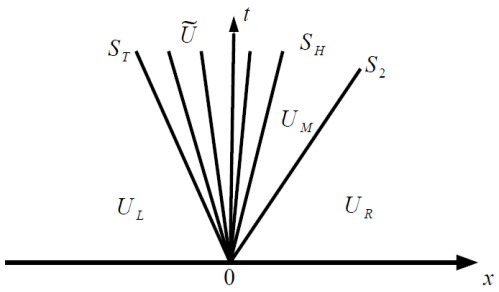

Figure 3.8: Possible rarefaction fan solution to the Riemann problem.

$i = 1, 2$) to represent the solution on our preferred $(\rho, \rho u)$ phase plane. In this case a phase transition will refer to the event of traffic changing from one state to another. Basically, the 1-Lax curve (2-Lax curve) is the set of points (loci) in the $(\rho, \rho u)$ phase plane, which can be connected to a given state by a 1-wave (2-wave). We state that the shock and rarefaction curves coincide for the Aw-Rascle system [8, 16]. Therefore to determine the 1-Lax curves, we arbitrary choose the situation where a given left state U_L can be connected to an arbitrary state U_* on the right by a 1-shock of speed S_1. This can only be admissible if the following entropy condition is satisfied

$$\lambda_1(\rho_*, u_*) < S_1 < \lambda_1(\rho_L, u_L).$$

Since any discontinuity propagating with speed S_1 satisfy the Rankine-Hugoniot condition [17, 30], we write;

$$\rho_* u_* - \rho_L u_L = S_1(\rho_* - \rho_L) \tag{3.75}$$
$$y_* u_* - y_L u_L = S_1(y_* - y_L) \tag{3.76}$$

Eliminating S_1 from (3.75) and (3.76) yields;

$$(y_* u_* - y_L u_L)(\rho_* - \rho_L) = (\rho_* u_* - \rho_L u_L)(y_* - y_L)$$

which simplifies to,

$$\frac{y_*}{\rho_*} = \frac{y_L}{\rho_L} \tag{3.77}$$

And since state U_* is arbitrary, the 1-Lax curve passing through U_L are obtained from (3.77) in terms of the primitive variables as;

$$L_1(\rho; \rho_L, u_L) = u_L + p(\rho_L) - p(\rho) \tag{3.78}$$

Note that in (3.77), the 1-wave is a shock if $\rho_L < \rho_*$ and a rarefaction if $\rho_L > \rho_*$. The 2-Lax curves are obtained by considering one of the Rankine Hugoniot condition (3.75), (3.76) and by stating that an arbitrary left state U_* can be connected to a given right state U_R by a contact discontinuity of speed S_2 if the following parallel characteristics condition [30] is satisfied;

$$\lambda_2(\rho_*, u_*) = \lambda_2(\rho_R, u_R) = S_2$$

Hence using (3.75) we write;

$$\rho_* u_* - \rho_R u_R = u_R(\rho_* - \rho_R) \tag{3.79}$$

whereby we deduce that $u_* = u_R$. Since U_* is arbitrary, then 2-Lax curves passing through U_R are given as;

$$L_2(\rho; \rho_R, u_R) = u_R. \tag{3.80}$$

That is they are straight lines exiting the origin in the $(\rho, \rho u)$ plane. Having obtained the 1-Lax curves and the 2-Lax curves, we now simply state the Riemann invariants w_1 and w_2 associated with the respective characteristic λ_1 and λ_2

$$w_1 = u + p(\rho) \quad , \qquad w_2 = u. \tag{3.81}$$

For numerical purpose (in the ensuing chapter) we present the solution, say U_G, to the Riemann problem (3.74) set at $x = 0$ as follows:

$$U_G = \begin{cases} U_M & if \quad S_1 < 0 \\ U_L & if \quad S_1 > 0 \\ \widetilde{U} & if \quad S_T < 0 < S_H \end{cases} \tag{3.82}$$

where the intermediate state $U_M = (\rho_M, y_M)^T$ is computed from the Lax curves as below:

$$u_M + p(\rho_M) = u_L + p(\rho_L) \tag{3.83}$$

Since $u_M = u_R$ and $y = \rho u + \rho p(\rho)$ we obtain from (3.83) the following expressions;

$$\begin{aligned} \rho_M &= p^{-1}(u_L + p(\rho_L) - u_R) \\ y_M &= \rho_M \frac{y_L}{\rho_L} \end{aligned} \tag{3.84}$$

Hence obtaining the explicit form of the intermediate state U_M in terms of U_L,U_R. To obtain the solution $\widetilde{U} = (\tilde{\rho}, \tilde{y})^T$ i.e. $\widetilde{U} = \widetilde{U}(U_L, U_M)$ inside the rarefaction fan, we consider the speed of the characteristic rays inside the fan, see figure 3.8 and also use Lax curves to have;

$$\begin{aligned} \tilde{u} + p(\tilde{\rho}) &= u_L + p(\rho_L) \\ \tilde{u} - \tilde{\rho} p(\tilde{\rho}) &= 0 \qquad\qquad \because \frac{x}{t} = 0. \end{aligned} \tag{3.85}$$

which upon solving simultaneously for $\tilde{\rho}$ and $\tilde{u}$ yields the desired form of the Riemann solution $\widetilde{U}$. To compute the speeds S_1,S_T and S_H we note that U_L and U_M can always be connected by a 1-rarefaction wave provided they lie on the same integral curve (on which rarefaction curves lie) and that the condition $\lambda_1(\rho_L, u_L) < \lambda_1(\rho_M, u_M)$ needs to be satisfied, see [17]. Otherwise, if $\lambda_1(\rho_L, u_L) > \lambda_1(\rho_M, u_M)$ then the two states should be connected by a 1-shock and so from the Rankine Hugoniot condition we have;

$$S_1 = \frac{\rho_L u_L - \rho_M u_M}{\rho_L - \rho_M}$$

Moreover, since the right(left) edge of the 1-rarefaction wave is said to carry the value $U_M(U_L)$ [30], we write;

$$\begin{aligned} S_T &= u_L - \rho_L p\prime(\rho_L) \\ S_H &= u_M - \rho_M p\prime(\rho_M) \end{aligned} \tag{3.86}$$

Finally, we illustrate on the $(\rho, \rho u)$ phase plane how the derived Aw-Rascle type traffic model (3.68)-(3.69) handles transitions from a left state U_L to the right U_R with the aid of the above determined i-Lax curves(for i=1,2). We sample two cases:

Case 1: $\rho_L = \rho_R$, $u_L > u_R$. This is shown in figure 3.9(a) whereby to reach U_R from U_L, the model predicts that traffic should first decelerate through 1-shock to state U_M along the outer 1-Lax curve, then transit from U_M to U_R along the lower 2-Lax curve(ray), while maintaining its average velocity.

Case 2: $\rho_L > \rho_R$, $u_L < u_R$. This is shown in figure 3.9(b). Herewith, to reach U_R from U_L, the model predicts that traffic first accelerates through 1-rarefaction fan to a new state $U_{\widehat{M}}$ situated along the inner 1-Lax curve and also on the upper 2-Lax curve(ray). Then transits from $U_{\widehat{M}}$ to U_R along the upper 2-Lax curve(ray).A detailed explanation and more representations on phase planes of solutions to the Aw-Rascle system with Riemann initial data can be found in [8]. See also [18] for more on phase transitions.

To conclude we include the relaxation term in the conservative form (3.68)-(3.69) of the macroscopic traffic models introduced in sections 3.1,3.2 and 3.3 as follows: we define the source term $S(U)$ as the vector;

$$S(U) = \begin{pmatrix} 0 \\ \\ \rho R(u, \rho) \end{pmatrix} \tag{3.87}$$

i.e. as a function of conservative variables ρ and y which are components of the vector $U = (\rho, y)^T$. The source term comprises of the relaxation term $R(u, \rho)$, that is expressed here in terms of the primitive variables ρ and u. Note that the velocity $u = y/\rho - p(\rho)$. The relaxation term can also be expressed in terms of

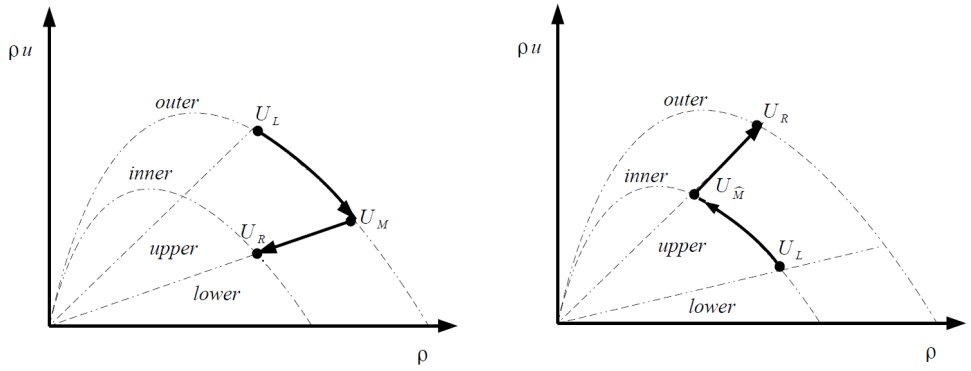

Figure 3.9: Illustration of traffic phase transitions with the aid of Lax curves. Shown in (a) is a 1-shock followed by a 2-contact, and in (b) is a 1-rarefaction followed by a 2-contact.

the conservative variables. However, its use in this form in (3.87) is equivalent to using $R(u, \rho)$. Hence we opt to use the latter. Now writing the conservative system (3.68)-(3.69) in vector form as it was done while introducing the Riemann problem in (3.74), and using (3.87) we obtain the following system

$$\partial_t U + \partial_x F(U) = S(U). \tag{3.88}$$

This is the conservative form of the traffic flow models (3.14),(3.52) with their respective relaxation term (3.15), (3.56) and (3.59) for the macroscopic Speed Adaptation, the Switching Curve and the modified Switching Curve models.

4 The Numerics

In this chapter we numerically investigate the ability of the macroscopic traffic models derived in the previous chapter to reproduce the features of 3-phase traffic theory. To this end, we simulate a multilane road that has a bottleneck. We regard a lane-drop as the stationary bottleneck and a slow moving vehicle(s) as a moving bottleneck. The simulation involves obtaining a numerical solution to the conservative system (3.88). We use a hybrid numerical scheme proposed in [16], that is based on the Godunov scheme to approximate shock and rarefaction waves, but uses a Glimm's random strategy to sample the contact discontinuity.

4.1 Outline of the Godunov Scheme

To numerically solve the homogeneous system:

$$\partial_t U + \partial_x F(U) = 0 \tag{4.1}$$

of (3.88), the spatial domain is discretized into M cells, $C_j = [x_{j-\frac{1}{2}}, x_{j+\frac{1}{2}}]$ for $j = 1 \cdots M$ of the same size Δx. The cell interfaces and cell center are respectively defined as $x_{j-\frac{1}{2}} = (j-1)\Delta x$, $x_{j+\frac{1}{2}} = j\Delta x$ and $x_j = (j-\frac{1}{2})\Delta x$. Moreover, discretization of the temporal domain is done in time intervals Δt, whose choice depends on the Courant-Friedrichs-Lewy(CFL) condition. Suppose that at time $t = t^n$, the general initial data for (4.1) is given as $\widetilde{U}(x, t^n)$. Then the first step of the Godunov scheme is the evolution of the solution to a time $t^{n+1} = t^n + \Delta t$. That is achieved through considering the cell averages,

$$U_j^n = \frac{1}{\Delta x} \int_{x_{j-\frac{1}{2}}}^{x_{j+\frac{1}{2}}} \widetilde{U}(x, t^n) dx \tag{4.2}$$

which now produces a piecewise constant approximation of the solution $U(x, t^n)$ as;

$$U(x, t^n) = U_j^n \qquad for\ all\ x \in C_j,\ j = 1 \cdots M,\ n \in \mathbb{N} \tag{4.3}$$

The second step is that of obtaining the solution for the local Riemann problems, say $RP(U_j^n, U_{j+1}^n)$, at the cell interface $x_{j+\frac{1}{2}}$ with data U_j^n and U_{j+1}^n, respectively, on

the left side and right side of position $x_{j+\frac{1}{2}}$. The solutions to this Riemann problem are self-similar solutions,

$$U_{j+\frac{1}{2}}(\tilde{x}/\tilde{t}), \qquad \tilde{x} = x - x_{j+\frac{1}{2}},\ \tilde{t} = t - t^n,\ x \in [x_j, x_{j+1}],\ t \in [t^n, t^{n+1}]$$

i.e. they are functions of the Riemann problem local coordinates $\tilde{x}/\tilde{t}$ and are constituted by the 1-and 2-waves. Now for a sufficiently small time step Δt, such that there are no wave interactions (see condition (4.6)), we obtain the global solution $\widetilde{U}(x,t)$ in the entire spatial domain, for $t \in [0, \Delta t]$, by gluing together the solutions of the local Riemann problems set at each interface of the cells as below,

$$\widetilde{U}(x,t) = U_{j+\frac{1}{2}}(\tilde{x}/\tilde{t}), \qquad for\ all\ (x,t) \in [x_j, x_{j+1}] \times [0, \Delta t] \tag{4.4}$$

Having obtained the solution $\widetilde{U}(x,t)$, the final step of the Godunov scheme entails the evolution of the solution to a time $t^{n+1} = t^n + \Delta t$ by defining a new set $\left\{U^n_{j+1}\right\}$ of average values as follows

$$U^{n+1}_j = \frac{1}{\Delta x} \int_{x_{j-\frac{1}{2}}}^{x_{j+\frac{1}{2}}} \widetilde{U}(x, t^{n+1}) dx \tag{4.5}$$

within $C_j = [x_{j-\frac{1}{2}}, x_{j+\frac{1}{2}}]$. To guarantee that the interaction of the i-waves, $i = 1, 2$ is entirely contained within cell C_j we impose the following CFL condition;

$$\Delta t \leq \frac{C_{cfl} \Delta x}{max\left\{|\lambda_i(U)|,\ i = 1, 2\right\}}. \tag{4.6}$$

C_{cfl} is called the Courant number and is usually set to 1. The CFL condition together with the integral form of the conservation law allows us to alternatively express U^{n+1}_j in the following form, see [17, 30]:

$$U^{n+1}_j = U^n_j + \frac{\Delta t}{\Delta x}\left[F^n_{j-\frac{1}{2}} - F^n_{j+\frac{1}{2}}\right] \tag{4.7}$$

with the intercell numerical flux given by;

$$F^n_{j+\frac{1}{2}} = F(U_{j+\frac{1}{2}}(0^-; U^n_j, U^n_{j+1}))$$

4.1.1 Godunov Scheme and Contact Wave Resolution

Here we present the failure of Godunov scheme to properly resolve contact waves that arise in the traffic model (3.88) as discussed in [16]. This failure is attributed to the fact that Godunov scheme does not obey the maximum principle property(see the maximum principle theorem in [16]) on the velocity u. To show this we consider the Riemann problem (3.74) with the left and right states, U_L and U_R respectively,

set up in a way that the solution to the Riemann problem is an isolated contact wave moving at a speed $S_2 > 0$. That is,

$$U(x,t) = \begin{cases} U_L & if \quad x < S_2 t \\ U_R & if \quad x > S_2 t \end{cases} \tag{4.8}$$

with $\rho_L > 0$, $\rho_R > 0$, $\rho_L \neq \rho_R$, but whereby $u_L = u_R = S_2$. From the first step of the Godunov scheme (4.2) with $n = 0$, the CFL condition(4.6) and given that $S_2 > 0$, the update formula (4.5) in the first time step yields, $U_j^1 = U_j^0$, if $j \neq 1$ and for $j = 1$, which is the index of the cell affected by the 2-wave from $x_{j-\frac{1}{2}}$, we will have;

$$\begin{aligned} \rho_1^1 &= \frac{1}{\Delta x}\int_0^{\Delta x} \rho(x, \Delta t)dx \\ y_1^1 &= \frac{1}{\Delta x}\int_0^{\Delta x} y(x, \Delta t)dx \end{aligned} \tag{4.9}$$

which leads to,

$$\begin{aligned} y_1^1 &= \frac{1}{\Delta x}\int_0^{\Delta x} (\rho u + \rho p(\rho))(x, \Delta t)dx \\ &= \frac{S_2}{\Delta x}\int_0^{\Delta x} \rho(x, \Delta t)dx + \frac{1}{\Delta x}\int_0^{\Delta x} \rho p(\rho)(x, \Delta t)dx \end{aligned} \tag{4.10}$$

due to the fact that velocity u is constant at $u_L = u_R = S_2$ across the contact wave. From (4.9) and (4.10) we get;

$$y_1^1 = S_2\rho_1^1 + \frac{1}{\Delta x}\int_0^{\Delta x} \rho p(\rho)(x, \Delta t)dx = S_2\rho_1^1 + (\rho p(\rho))_1^1 \tag{4.11}$$

Now calculating the velocity u_1^1 from ρ_1^1 and y_1^1 and considering the result (4.11) we get;

$$u_1^1 = \frac{y_1^1}{\rho_1^1} - p(\rho_1^1) = S_2 + \frac{(\rho p(\rho))_1^1 - \rho_1^1 p(\rho_1^1)}{\rho_1^1}$$

As a result of the convexity of the function $\rho \to \rho p(\rho)$, and by Jensen's inequality it follows that $(\rho p(\rho))_1^1 \geq \rho_1^1 p(\rho_1^1)$. Hence;

$$u_1^1 \geq S_2 (= u_L = u_R)$$

that is after the first time step, the velocity will not be equal everywhere in the spatial domain. Hence the Godunov scheme fails to resolve contact waves correctly.

4.2 A Hybrid Scheme for Contact Wave

We now present the algorithm proposed in [16], that resolves the above stated deficiency of the Godunov scheme. The idea of the algorithm is to keep on using the Godunov scheme to resolve shock and rarefaction waves (which it does very well), but use a Glimm's random sampling technique [29, 30] to properly capture the contact waves. Therefore the algorithm is presented in two steps. We start with how the sampling is done in order to take into account only the contact waves. We consider an interval $[x_{j-1}, x_{j+1}]$, $j = 1 \cdots M$ upon which the Riemann problem on the interfaces $x_{j-\frac{1}{2}}$ and $x_{j+\frac{1}{2}}$ is set. Note that under the CFL condition (4.6) the Riemann problem set at other interfaces outside the interval $[x_{j-1}, x_{j+1}]$ do not influence the solution U_j^{n+1}. So U_j^{n+1} only depends on the three states, U_{j-1}^n, U_j^n,and U_{j+1}^n. To proceed, we state that the Riemann problem at the interfaces $x_{j-\frac{1}{2}}$ and $x_{j+\frac{1}{2}}$ give rise in general to a 1-wave and a 2-wave (in this case a 2-contact that propagates at speed $S_2 = u > 0$) as shown in figure 4.1 below;

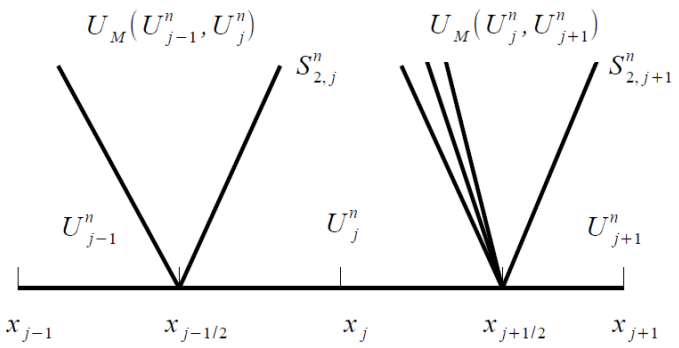

Figure 4.1: The considered interval $[x_{j-1}, x_{j+1}]$

As in [16], the solution $\widetilde{U}(x, t^{n+\frac{1}{2}})$ at $t^{n+\frac{1}{2}}$ and on interval $[x_{j-1}, x_{j+1}]$ is defined as a piecewise constant function on each subinterval $[x_{j-1}, x_{j-\frac{1}{2}})$, $[x_{j-\frac{1}{2}}, x_{j+\frac{1}{2}})$, and $[x_{j+\frac{1}{2}}, x_{j+1}]$. This function randomly picks up a value between U_{j-1}^n, $U_M(U_{j-1}^n, U_j^n)$, U_j^n, $U_M(U_j^n, U_{j+1}^n)$ and U_{j+1}^n as per their rate of occurrence in their respective subintervals. That is;

$$\widetilde{U}(x, t^{n+\frac{1}{2}}) = \begin{cases} U_{j-1}^n & if \quad x \in [x_{j-1}, x_{j-\frac{1}{2}}) \\ U_j^{n+\frac{1}{2}} & if \quad x \in [x_{j-\frac{1}{2}}, x_{j+\frac{1}{2}}) \\ U_{j+1,L}^{n+\frac{1}{2}} & if \quad x \in [x_{j+\frac{1}{2}}, x_{j+1}] \end{cases} \tag{4.12}$$

with

$$U_j^{n+\frac{1}{2}} = \begin{cases} U_M(U_{j-1}^n, U_j^n) & if \quad a_{n+1} \in (0, \frac{\Delta t}{\Delta x} S_{2,j}^n) \\ U_j^n & if \quad a_{n+1} \in [\frac{\Delta t}{\Delta x} S_{2,j}^n, 1) \end{cases} \tag{4.13}$$

and

$$U_{j+1,L}^{n+\frac{1}{2}} = \begin{cases} U_M(U_j^n, U_{j+1}^n) & if \quad a_{n+1} \in (0, \frac{2\Delta t}{\Delta x} S_{2,j}^n) \\ U_{j+1}^n & if \quad a_{n+1} \in [\frac{2\Delta t}{\Delta x} S_{2,j}^n, 1) \end{cases} \tag{4.14}$$

The random sampling technique in (4.13) and (4.14) is achieved via the van der Corput random sequence (a_n) within the interval (0,1) and defined as below [29, 30];

$$a_n = \Sigma_{k=0}^L i_k 2^{-(k+1)} \quad , \quad n = \Sigma_{k=0}^L i_k 2^k$$

with $i_k = 0, 1$ being the binary expansion of the integers $n = 1, 2, \cdots$.

The second step of the algorithm involves taking into account the shock and rarefaction waves in the solution to the Riemann problems. This is the step that involves the Godunov scheme. We begin this step by considering the Riemann problem set at $x_{j+\frac{1}{2}}$. The part of its solution that has influence on cell $C_j = [x_{j-\frac{1}{2}}, x_{j+\frac{1}{2}}]$ is located on the left of the contact wave emanating from interface $x_{j+\frac{1}{2}}$, and obtained by averaging $\widetilde{U}(.; U_j^{n+\frac{1}{2}}, U_{j+1,L}^{n+\frac{1}{2}})$ on $(x_j, x_{j+\frac{1}{2}})$, which is equivalent to the average;

$$U_{j+\frac{1}{2},L}^{n+1} = \frac{2}{\Delta x} \int_{x_j}^{x_{j+\frac{1}{2}}} \widetilde{U}\left(\frac{x - x_{j+\frac{1}{2}}}{\Delta t}; U_j^{n+\frac{1}{2}}, U_{j+1}^n\right) dx \tag{4.15}$$

This is because $U_{j+1,L}^{n+\frac{1}{2}}$ and U_{j+1}^n are either equal or separated by a 2-contact. Now consider the Riemann problem set at $x_{j-\frac{1}{2}}$. The part of its solution that has influence on cell C_j is obtained by averaging $\widetilde{U}(.; U_{j-1}^n, U_j^{n+\frac{1}{2}})$ on $[x_{j-\frac{1}{2}}, x_j)$.This solution is located on both sides (i.e. on the left and right) of the 2-contact, if this type of 2-wave is present at the interface $x_{j-\frac{1}{2}}$. Hence we can write these three possibilities, see [16]:

- For the right side of the 2-contact in $\widetilde{U}(.; U_{j-1}^n, U_j^{n+\frac{1}{2}})$ where the random sampling makes the choice,

$$U_j^{n+\frac{1}{2}} = U_j^n \quad with \quad U_M(U_{j-1}^n, U_j^n) \neq U_j^n \tag{4.16}$$

  we replace U_{j-1}^n by $U_j^{n+\frac{1}{2}}$ in the $\widetilde{U}$ to have;

$$U_{j-\frac{1}{2},R}^{n+1} = \frac{2}{\Delta x} \int_{x_{j-\frac{1}{2}}}^{x_j} \widetilde{U}\left(\frac{x - x_{j-\frac{1}{2}}}{\Delta t}; U_j^{n+\frac{1}{2}}, U_j^{n+\frac{1}{2}}\right) dx = U_j^{n+\frac{1}{2}} \tag{4.17}$$

- For the left side of the 2-contact in $\widetilde{U}(.;U_{j-1}^{n},U_{j}^{n+\frac{1}{2}})$ where now the random sampling choose;

$$U_{j}^{n+\frac{1}{2}}=U_{M}(U_{j-1}^{n},U_{j}^{n})\quad with\quad U_{M}(U_{j-1}^{n},U_{j}^{n})\neq U_{j}^{n} \tag{4.18}$$

we obtain the solution as the average;

$$U_{j-\frac{1}{2},R}^{n+1}=\frac{2}{\Delta x}\int_{x_{j-\frac{1}{2}}}^{x_{j}}\widetilde{U}\left(\frac{x-x_{j-\frac{1}{2}}}{\Delta t};U_{j-1}^{n},U_{j}^{n+\frac{1}{2}}\right)dx \tag{4.19}$$

Since that the condition $U_{M}(U_{j-1}^{n},U_{j}^{n})\neq U_{j}^{n}$ in (4.16) and (4.18) is equivalent to $U_{M}(U_{j-1}^{n},U_{j}^{n+\frac{1}{2}})\neq U_{j}^{n+\frac{1}{2}}$ if $U_{j}^{n+\frac{1}{2}}=U_{j}^{n}$, we can collectively write;

$$U_{j-\frac{1}{2},R}^{n+1}=\begin{cases}\frac{2}{\Delta x}\int_{x_{j-\frac{1}{2}}}^{x_{j}}\widetilde{U}\left(\frac{x-x_{j-\frac{1}{2}}}{\Delta t};U_{j-1}^{n},U_{j}^{n+\frac{1}{2}}\right)dx;\\ \qquad\qquad if\quad U_{M}(U_{j-1}^{n},U_{j}^{n+\frac{1}{2}})=U_{j}^{n+\frac{1}{2}}\\ U_{j}^{n+\frac{1}{2}};\\ \qquad\qquad otherwise\end{cases} \tag{4.20}$$

- When within the time step Δt no 2-contact is present at interface $x_{j-\frac{1}{2}}$, then $U_{M}(U_{j-1}^{n},U_{j}^{n})=U_{j}^{n}$ and consequently $U_{j}^{n+\frac{1}{2}}=U_{j}^{n}$. Thus the solution $U_{j-\frac{1}{2},R}^{n+1}$ entering cell C_j is averaged as in the Godunov scheme:

$$U_{j-\frac{1}{2},R}^{n+1}=\frac{2}{\Delta x}\int_{x_{j-\frac{1}{2}}}^{x_{j}}\widetilde{U}\left(\frac{x-x_{j-\frac{1}{2}}}{\Delta t};U_{j-1}^{n},U_{j}^{n}\right)dx \tag{4.21}$$

Now combining the above averages of the Riemann solution on the half-cells $[x_{j-\frac{1}{2}},x_{j})$ and $(x_{j},x_{j+\frac{1}{2}}]$ we write the numerical solution at the next time step t^{n+1} as below

$$\begin{aligned}U_{j}^{n+1}&=\frac{1}{2}\left(U_{j+\frac{1}{2},L}^{n+1}+U_{j-\frac{1}{2},R}^{n+1}\right)\\&=U_{j}^{n+\frac{1}{2}}-\frac{\Delta t}{\Delta x}\left(F_{G,j+\frac{1}{2}}^{n+\frac{1}{2},L}-F_{G,j-\frac{1}{2}}^{n+\frac{1}{2},R}\right).\end{aligned} \tag{4.22}$$

The left and right numerical flux function are respectively given by;

$$F_{G,j+\frac{1}{2}}^{n+\frac{1}{2},L}=F_{G}(U_{j}^{n+\frac{1}{2}},U_{j+1}^{n})=F(U_{G,j+\frac{1}{2}}^{n+\frac{1}{2},L}).$$

$$F_{G,j-\frac{1}{2}}^{n+\frac{1}{2},R}=\begin{cases}F_{G}(U_{j-1}^{n},U_{j}^{n+\frac{1}{2}})=F(U_{G,j-\frac{1}{2}}^{n+\frac{1}{2},R});\\ \qquad\qquad if\quad U_{M}(U_{j-1}^{n},U_{j}^{n+\frac{1}{2}})=U_{j}^{n+\frac{1}{2}}\\ F(U_{j}^{n+\frac{1}{2}});\\ \qquad\qquad otherwise\end{cases}$$

with U_G computed as in section 3.4. Details on the properties of this numerical scheme can be found in [16].

To complete the numerical solution to the conservative system (3.88) we use the source term splitting approach [30] or the fractional step approach [17]. To this aim, letting $[x_0, x_M]$ to be the spatial domain, we state that given the initial value problem:

$$\begin{cases} \partial_t U + \partial_x F(U) = S(U), \quad x_0 \leq x \leq x_M \\ U(x, t^n) = U^n \end{cases} \tag{4.23}$$

The idea is to evolve U^n from time $t = t^n$ to the new value U^{n+1} at time $t = t^{n+1}$ in a time step $\Delta t = t^{n+1} - t^n$, that satifsy the CFL condition (4.6), by first solving the homogeneous system;

$$\begin{cases} \partial_t U + \partial_x F(U) = 0, \\ U(x, t^n) = U^n \end{cases} \qquad \Longrightarrow \overline{U}^{n+1} \tag{4.24}$$

using the hybrid numerical scheme (4.22) in a time step of size Δt to obtain the solution $\overline{U}^{n+1}$. Note that the initial condition for the homogeneous system (4.24) is the same initial condition for the non-homogeneous system (4.23). The second step of this approach is done by using $\overline{U}^{n+1}$ as the initial condition to solve the following ordinary differential equation that accounts for the presence of the source term;

$$\begin{cases} \dfrac{dU}{dt} = S(U), \\ \\ \overline{U}^{n+1}, \end{cases} \qquad \Longrightarrow U^{n+1} \tag{4.25}$$

and done in the same time step of size Δt (satisfying the condition (4.6)) to now obtain the approximate solution U^{n+1} of the non-homogeneous initial value problem (4.23) that is the discrete version of conservative system (3.88). The numerical method employed to solve (4.25) is the explicit Euler method;

$$U^{n+1} = U^n + \Delta t S(t^n, U^n), \quad \Delta t = t^{n+1} - t^n$$

where now $U^n \approx U(t^n)$. Hence the complete numerical scheme of the conservative system (3.88).

4.3 Numerical Tests of the Hybrid Scheme

In order to visualize the features of the numerical scheme presented in the previous section, we simulate the Aw-Rascle type macroscopic traffic model given by equations (3.68),(3.69) i.e. the derived model equations without the source term (i.e. the

relaxation term). Following the particular choice of the speed adaptation coefficient in equation (3.6), we take $p(\rho) = Cln(\frac{\rho}{1-\rho})$ in equation (3.69). We investigate two traffic flow scenarios that are envisaged in two Riemann problems. This in turn lead to two solutions of interest, namely: a 1-shock wave followed by a 2-contact wave and a 1-rarefaction wave followed by a 2-contact wave. In this case we choose $C = 0.7$ and the mesh size Δx as given in table 4.1, and consider the following Riemann problem, given in terms of the primitive variables:

$$V(x,0) = \begin{cases} V_L & if \quad x < x_0 \\ V_R & if \quad x > x_0 \end{cases} \tag{4.26}$$

where the left $V_L = (\rho_L, u_L)^T$ and the right $V_R = (\rho_R, u_R)^T$ traffic states are chosen as:

- Case 1:

$$\begin{aligned} \rho_L &= 0.4, \quad u_L = 1 \\ \rho_R &= 0.4, \quad u_R = 0.2 \end{aligned}$$

  with $x_0 = 0$. In this case the exact solution is given by a 1-shock wave followed by a 2-contact wave. Equations (3.84) can be used to obtain the exact solution. The results are shown in figure (4.2).

- Case 2:

$$\begin{aligned} \rho_L &= 0.6, \quad u_L = 0.05 \\ \rho_R &= 0.5, \quad u_R = 0.9 \end{aligned}$$

  with $x_0 = 0$. Here too, equations (3.84),(3.85) can be use to obtain the exact solution as a 1-rarefaction wave followed by a 2-contact wave. The results are shown in figure (4.3).

Note that in both cases the computation is done using the conservative variables ρ and $y = \rho u + \rho p(\rho)$. This is essential especially for determination of the correct intermediate state in Case 1.

Remark 4.3.1. *As proved in [16] for the consistency theorem, Theorem 3.1 part (iii), if only shock and rarefaction waves arise in the considered flow; then the hybrid scheme (4.22) coincides with the Godunov scheme. Therefore, for simulations done in the following section, we essentially use the Godunov scheme since the emergent congested traffic patterns are basically composed of shock and rarefaction waves.*

4.4 Simulation of 3-Phase Traffic Flow Features

We now introduce the source term (i.e.the relaxation term) to the conservative system (3.68)-(3.69) in order to proceed with our simulation of 3-phase traffic flow

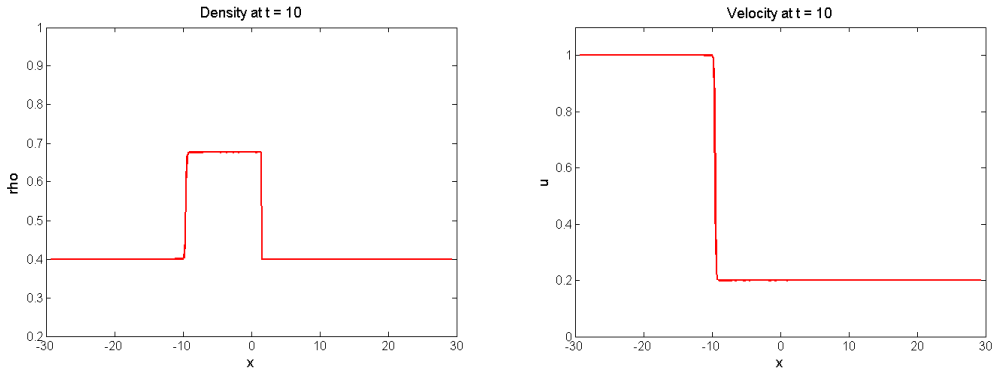

(a) (b)

Figure 4.2: The hybrid scheme solution to the Riemann problem; $\rho_L = 0.4, u_L = 1, \rho_R = 0.4, u_R = 0.2$ and $x_0 = 0$

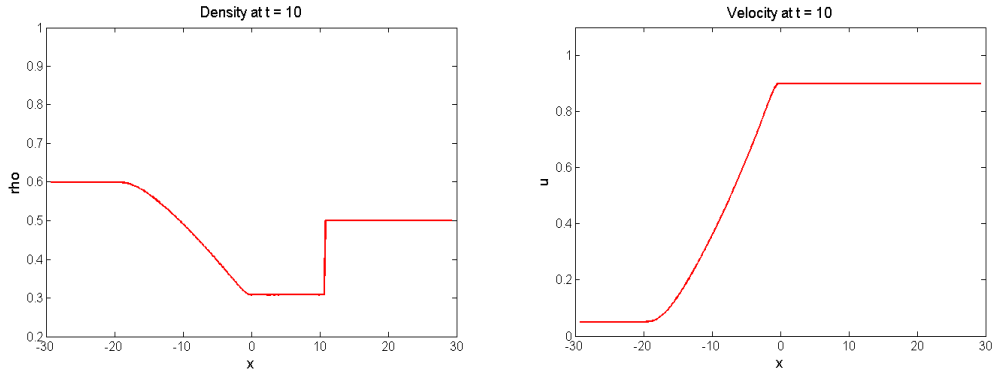

(a) (b)

Figure 4.3: The hybrid scheme solution to the Riemann problem; $\rho_L = 0.6, u_L = 0.05, \rho_R = 0.5, u_R = 0.9$ and $x_0 = 0$

features. To this end, we consider the non-homogeneous system 3.88 and the numerical scheme presented in section 4.2.

4.4.1 Traffic Breakdown at Road Bottlenecks

The kind of bottleneck that we consider in these simulations is a lane-drop, from 3 lanes to 2 lanes in a highway as shown in figure 4.4. It is well-known that any carriageway capacity is commensurate with the number of lanes it possess. Therefore the section of the highway with 3 lanes accommodates more vehicles than the part

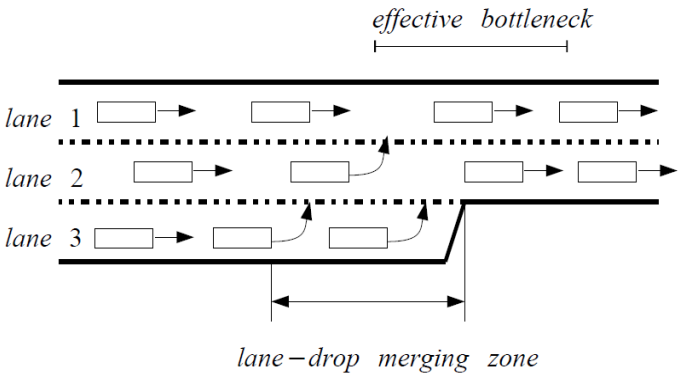

Figure 4.4: A lane-drop bottleneck.

with 2 lanes. As a consequence, the lane-aggregate maximal density of the section of the highway with 3 lanes is greater than that of the section of highway with 2 lanes. This is to mean that at an increased flow rate, the maximum capacity in the 2-lane section of the highway will be reached faster as the traffic from the third lane merge onto the other two lanes. This will in turn affect (negatively) the free flow of traffic and so congestion will set in at the location of lanes reduction. We will come back to onset of congestion shortly. We now look at how the effects of lane-drop are taken into account in the relaxation term, which is utilized in Chapter 2 to constitute the hypothesis of 3-phase traffic theory in the macroscopic traffic models derived therein. Let the highway under consideration be along the x-axis and beginning at $x = -50$ and ending at $x = 10$ with the lane-drop merging zone situated around $x = 0$. Let the direction of flow of traffic be in the direction of increasing x along the axis. Now suppose $\varphi(x)$ is a function representing the change in traffic density, due to the presence of the lane-drop, and satisfy the following;

(a) $1 \leq |\varphi(x)| \leq \eta$ for any $x \in [-50, 10]$.

(b) $\varphi(x) = 1$ in $(-50, -\delta)$ for $\delta > 0$.

(c) $\varphi(x) = \eta$ in $(\delta, 10)$.

(d) $\varphi(x)$ increases on $(-\delta, \delta)$.

as depicted in figure 4.5. Next we scale the density with this function $\varphi = \varphi(x)$ in the relaxation terms (3.15), (3.56) and (3.59) i.e.

$$R(u, \rho, \varphi) \quad = \quad \frac{1}{T}(U^e(\varphi\rho, u) - u) \tag{4.27}$$

with $U^e(.)$ given by the respective expressions characterizing the three macroscopic traffic models to be compared, i.e. the Switching Curve (SC), macroscopic Speed Adaptation (SA), and the modified Switching Curve (mod.SC) models. In the ensuing simulations we use the parameters given in tables 3.1 and 4.1.

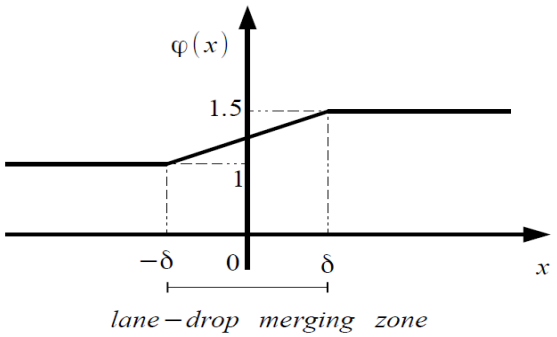

Figure 4.5: Function $\varphi(x)$ with $\eta = 3/2$ and $\delta = 1$.

Table 4.1: Model parameters used in simulations.

Δx	60/400	C_{cfl}	0.9
δ	1	η	3/2
C	0.3	T	5

Remark 4.4.1. *In [31], it has been shown that indeed the empirical flow-density diagram strongly depends both on the highway location where the diagram is measured and on the type of spatiotemporal congested traffic pattern present at the measurement location.*

We now resume the onset of congestion issue and demonstrate the ability of the macroscopic 3-phase traffic flow models to reproduce the empirically observed first-order $F \rightarrow S$ phase transition at road bottlenecks. The above stated road-inhomogeneity causes a permanent disturbance of traffic flow, localized in the neighborhood of the lane-drop. This is because there is merging of traffic from the ending lane 3 onto the two continuing lanes 1 and 2, figure 4.4, which happens within the lane-drop zone. Therefore, this disturbance of flow is permanent and localized i.e. it is a *deterministic disturbance*. A deterministic disturbance in free flow at the lane-drop bottleneck happens if: firstly, there is a high enough flow rate in free flow on the highway upstream of the lane-drop bottleneck, and secondly, vehicles merging from lane 3 onto the other two lanes (i.e. lanes 1 and 2) compel the vehicles on these two lanes to decelerate in the vicinity of the lane-drop zone. As a consequence of this deceleration, there will be a dynamic decrease in (lane-aggregated) velocity and in turn an increase in the (lane-aggregated) density localized in the vicinity of the bottleneck as shown in figures 4.6(a)-(f). As more vehicles perform the mandatory lane changes from lane 3 to merge onto lanes 1 and 2, and also due to the high enough flow rate; the amplitude of the deterministic disturbance will grow. However, this growth has a limit which is the *nucleus* required for the oc-

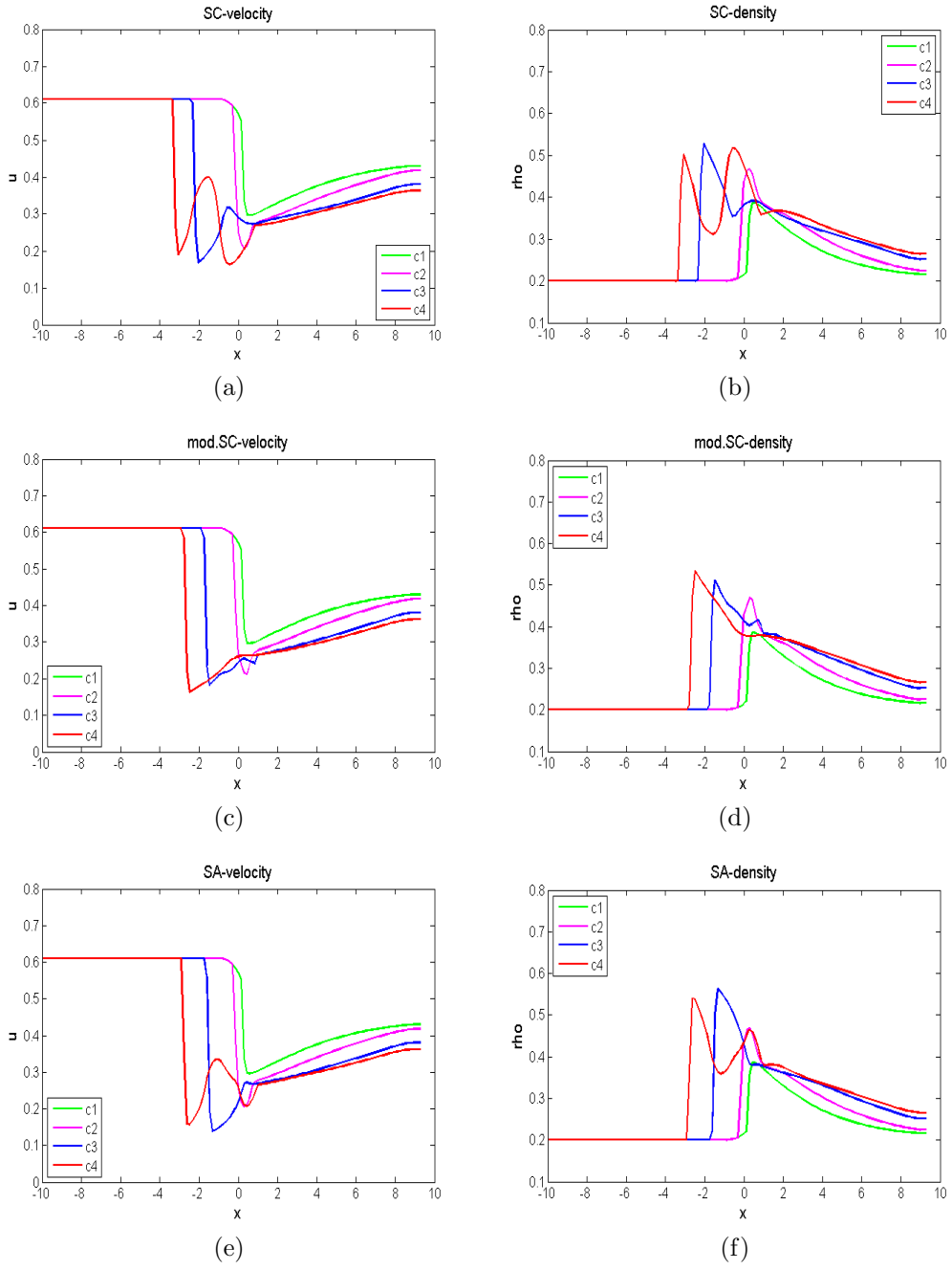

Figure 4.6: Simulation of velocity, u and density, ρ dynamic changes within the deterministic disturbance at the lane-drop bottleneck. The curves $c1-c4$ are related to different time moments.

currence of traffic breakdown i.e. $F \rightarrow S$ transition. If this limit is exceeded then

$F \rightarrow S$ transition occurs at the bottleneck, compare curves $c2$ and $c3$ in figures 4.6(a)-(f). The deterministic disturbance in initial free flow becomes a nucleus for traffic breakdown if within this disturbance the velocity decreases to or below the critical velocity required for $F \rightarrow S$ transition, respectively, the density increases to or above the critical density [1]. Now with increased flow rate at the bottleneck due to merging of vehicles, a wave of dense traffic appears and propagates upstream, see curve $c4$ in figures 4.6(a)-(f). The curve $c4$ in figures 4.6(a),(b),(e) and (f) shows a narrow moving jam already propagating upstream. Note that the formation of the wave of dense traffic begins with the upstream propagation of the upstream front of the deterministic disturbance at a velocity that increases with increase of vehicle merges. After the downstream front of the wave appears within the disturbance and propagates upstream, then the upstream front of this wave will now tend to conform its propagation velocity to the velocity at which the downstream front propagates. Generally, as shown in figures 4.6(a)-(f), the Switching Curve (SC), modified Switching Curve (mod.SC) and macroscopic Speed Adaptation (SA) models predicts that, after the occurrence of a $F \rightarrow S$ transition at the lane-drop bottleneck, moving jams emerges and propagates upstream.

In the flow-density plane, see figure 4.7, the flow rate within the deterministic disturbance increases with an increase of the density that is in turn a result of a decrease in the velocity within this disturbance. However, due to the merging of vehicles at the lane-drop, this increase in the disturbance reaches a limit upon which the velocity within the disturbance decreases and density increases abruptly leading to a $F \rightarrow S$ transition. Thus synchronized flow emerges. In particular, there appears a moving synchronized flow pattern (MSP) i.e. an upstream propagating narrow moving jam that is surrounded both upstream and downstream by free flow. As a result of the upstream propagation of the downstream front of synchronized flow, that was initially fixed at the bottleneck, there will be an increase in velocity within the deterministic disturbance. This velocity increase has some limit upon which the velocity of vehicles in synchronized flow increases and density decreases drastically. Thus leading to a return to free flow at the lane-drop bottleneck. Hence, a $S \rightarrow F$ phase transition occurs, completing a loop i.e. a hysteresis loop where the upper part of the loop is the deceleration branch associated with $F \rightarrow S$ transition while the lower part of the loop is the acceleration branch associated with a $S \rightarrow F$ transition. However, this free flow traffic state exists for only a short period of time and then another $F \rightarrow S$ transition occurs spontaneously at the bottleneck leading to a new moving synchronized flow pattern (MSP). See curve $c4$ in figures 4.6(a)-(f). Eventually we will observe a sequence of MSPs.

4.4.2 Spatiotemporal Congested Traffic Patterns

In the previous section 4.4.1, the nature of traffic breakdown phenomenon at a highway bottleneck (in particular a lane-drop) has been discussed. We have showed

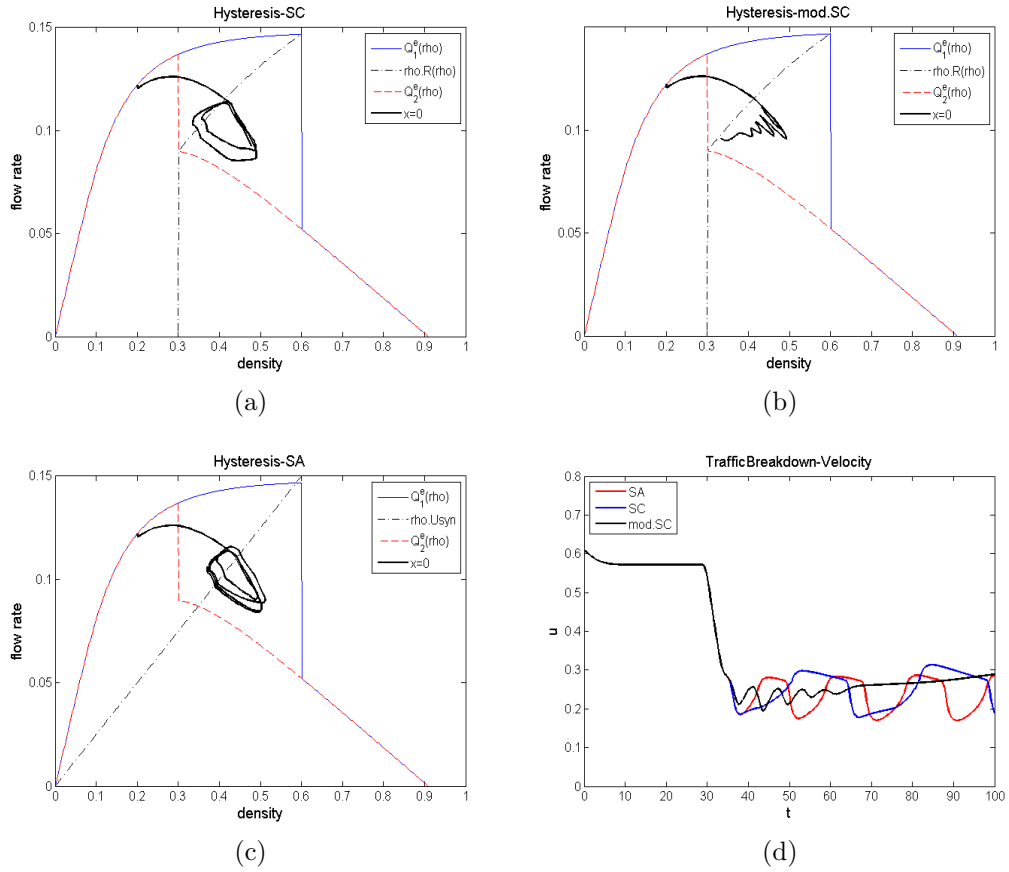

Figure 4.7: (a)-(c) Traffic hysteresis effects at the lane-drop merging zone, depicted in the flow-density plane. (d) The time dependence of the velocity u within the deterministic disturbance at the lane-drop bottleneck.

the capability of the three models to reproduce the empirically observed spontaneous appearance of a deterministic disturbance at the bottleneck and whose amplitude grow to exceed some critical value leading to a spontaneous $F \rightarrow S$ phase transition.

In this section we look into the above featured models' ability to replicate the observed features of spatiotemporal congested patterns that occur in a highway once traffic breakdown has occurred at the highway bottleneck(s). In [32], its is shown that synchronized flow pattern (SP) and *general* pattern (GP) of congested traffic occurs in the vicinity of an isolated bottleneck(i.e. an effective bottleneck located far enough from other effective bottlenecks on the considered highway). A general pattern (GP) is a spatiotemporal congested traffic pattern consisting of synchronized flow that borders the isolated bottleneck location but this synchronized flow is in turn bordered upstream by a sequence of wide moving jams. After traffic breakdown is realized at an isolated bottleneck, various patterns of synchronized

flow may result. These patterns are differentiated by the behavior of their upstream and downstream fronts that separate the synchronized flow within, from the free flow outside of the congested traffic. As pointed out earlier, in section 2.1 a SP can either be a localized SP (LSP), moving SP (MSP) or a widening SP (WSP). We take the lane-drop set-up depicted in figure 4.4, to be our isolated bottleneck and investigate the kind of synchronized flow patterns, discussed in [1], that the Switching Curve, modified Switching Curve and the macroscopic Speed Adaptation models are able to reproduce at the bottleneck location. As shown in figure 4.8, the macroscopic

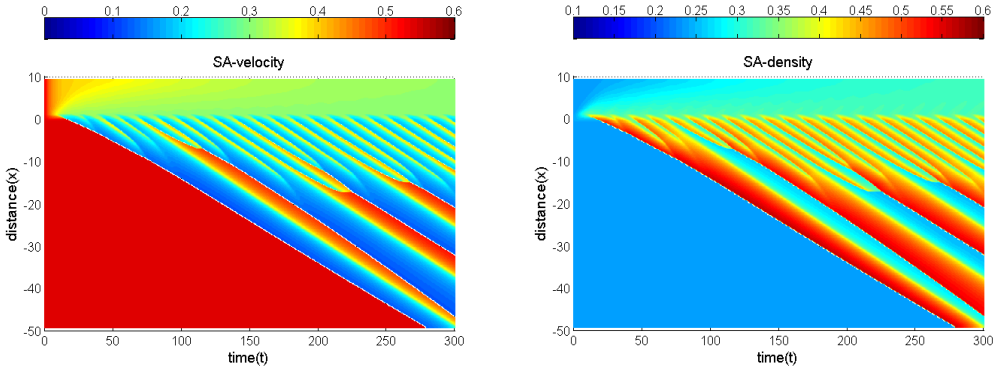

(a) (b)

Figure 4.8: Spatiotemporal congested traffic patterns simulation with macroscopic Speed Adaptation (SA) model.

Speed Adaptation model produces MSPs. Also, in figure 4.9 the modified Switching

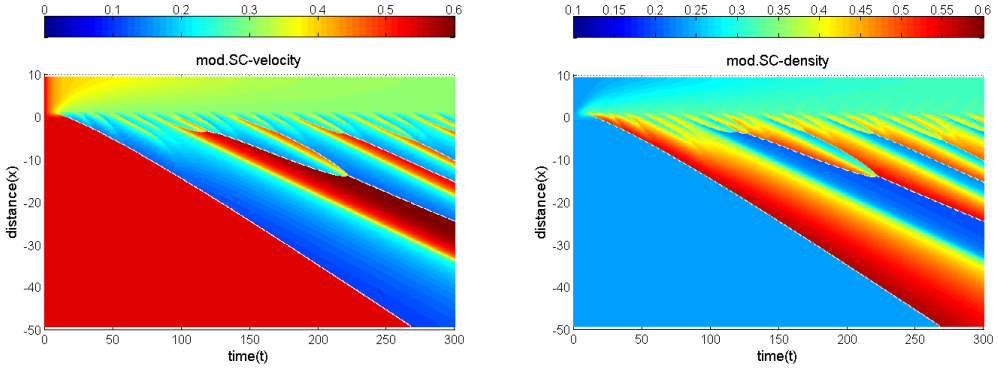

(a) (b)

Figure 4.9: Spatiotemporal congested traffic patterns simulation with modified Switching Curve (mod.SC) model.

Curve model is shown to produce MSPs, which do not extend upstream of the bottleneck like in the SA model. These MSPs or rather narrow jams grow (i.e. velocity decrease and density increase within them) as they move upstream of the lane-drop bottleneck. As discussed in [32, 24], a phenomenon of growing narrow

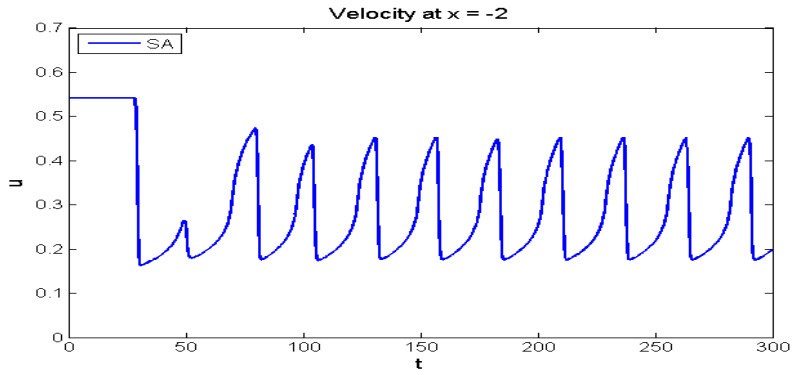

Figure 4.10: Narrow moving jams propagation at location $x = -2$ for the macroscopic Speed Adaptation model.

jams is that if two or more growing narrow moving jams are relatively close to a one another and one of these narrow jams grow into a wide moving jam, then the further growth of the narrow jams that are nearby is suppressed and/or they merge with the wide jam that has been formed. Hence a $S \rightarrow J$ phase transition is realized. Moreover, if growing narrow moving jams are far enough from the wide moving jam, then the process of either suppressing and/or merging of these narrow jams result into another wide jam formation. This is vividly shown in figures 4.8 and 4.11 whereby the growing narrow moving jams at $x = -2$ in figure 4.10, merge later on, see for example at $x = -10$, to transform into wide moving jams at $x = -14$. In the course of formation of these narrow moving jams, the downstream front start to propagate upstream from the lane-drop bottleneck. As a result, the velocity(density) within the deterministic disturbance increases(decreases) past the limit necessary for sustainment of synchronized flow leading to a return to free flow at the bottleneck. However this free flow state is short-lived and so another traffic breakdown occurs at the bottleneck and in turn another upward moving narrow jam emerges. This process is repeated resulting to a sequence of narrow moving jams of low velocity within them, figures 4.8 and 4.9. Looking at the simulation results of the Switching Curve model, figure 4.12 reveals that this model is not quite a 3-phase traffic flow model. In particular, the onset of congestion at the lane-drop, for this model leads to formation of moving jams that are rather wide and are such that the velocity within them decline rapidly, hence readily forming wide moving jams. Figure 4.13 shows the flow-density relations at various location of the considered highway, i.e. upstream of the lane-drop,$x = -20$, within the lane-drop,$x = 0$, and downstream of the lane-

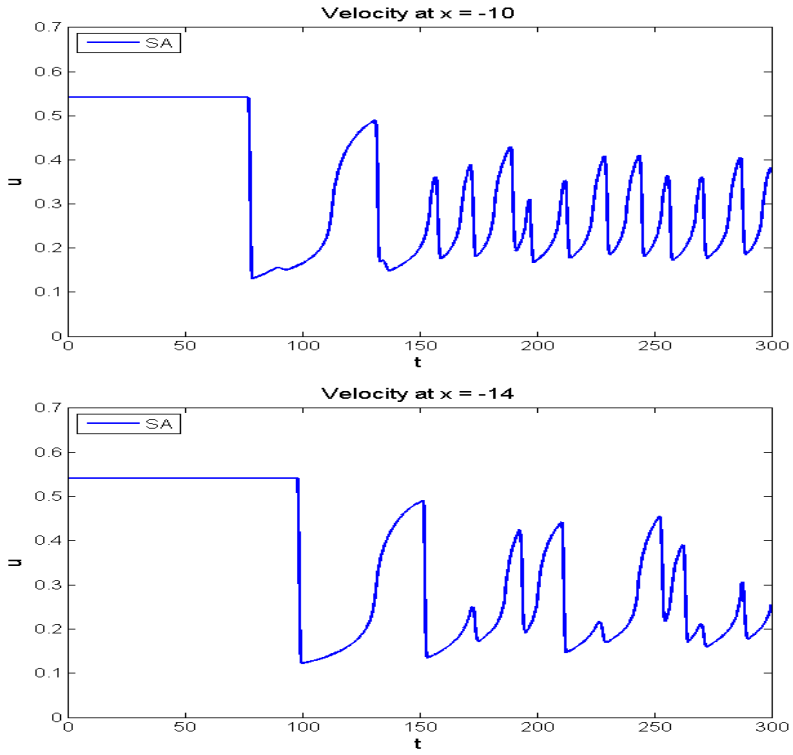

Figure 4.11: Narrow moving jams propagation at $x = -10$ and coalescence at location $x = -14$ for the macroscopic Speed Adaptation model.

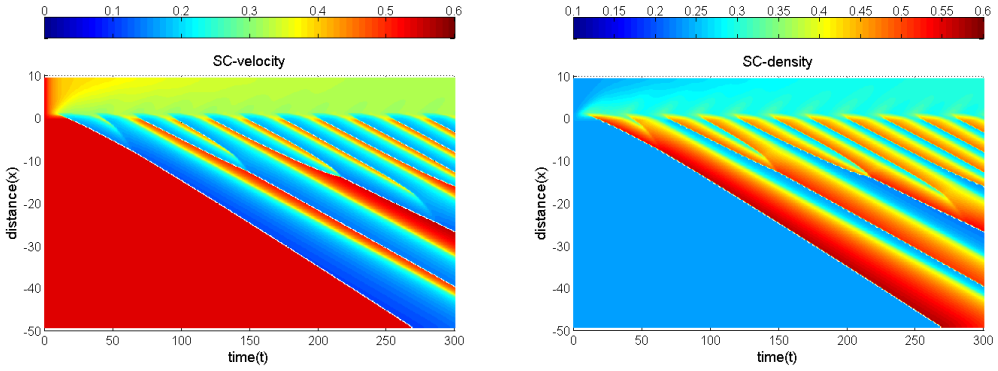

(a) (b)

Figure 4.12: Spatiotemporal congested traffic patterns simulation with Switching Curve(SC) model.

drop,$x = 5$. Due to the high flow rate on the 3-lane highway section upstream of the lane-drop and the lane-drop itself, the highway section downstream of the lane-

drop i.e. the 2-lane section operates at maximum capacity. This is depicted by the simulation data points for highway location $x = 5$ on the flow-density plane scaled-down by a factor $\frac{2}{3}$. Within the lane-drop location i.e. $x = 0$ synchronized flow, that is MSP, is reported for the modified Switching Curve (mod.SC) and the macroscopic Speed Adaptation (SA) models. For the Switching Curve (SC) model at the same location,$x = 0$, shown in figure 4.14(a) the traffic hysteresis loop is pronounced, unlike in the mod.SC and SA models. Thus we can state that the SC model rather predicts a $F \to J$ transition rather than a $F \to S$ transition captured by the other two models, which produces moving synchronized flow pattern. Upstream of the lane-drop i.e. $x = -20$, wide moving jams propagate through free flow. These wide moving jams possess the characteristic feature of maintaining the velocity of the downstream front that is approximately -20 km/h, see figures 4.13 and 4.14.

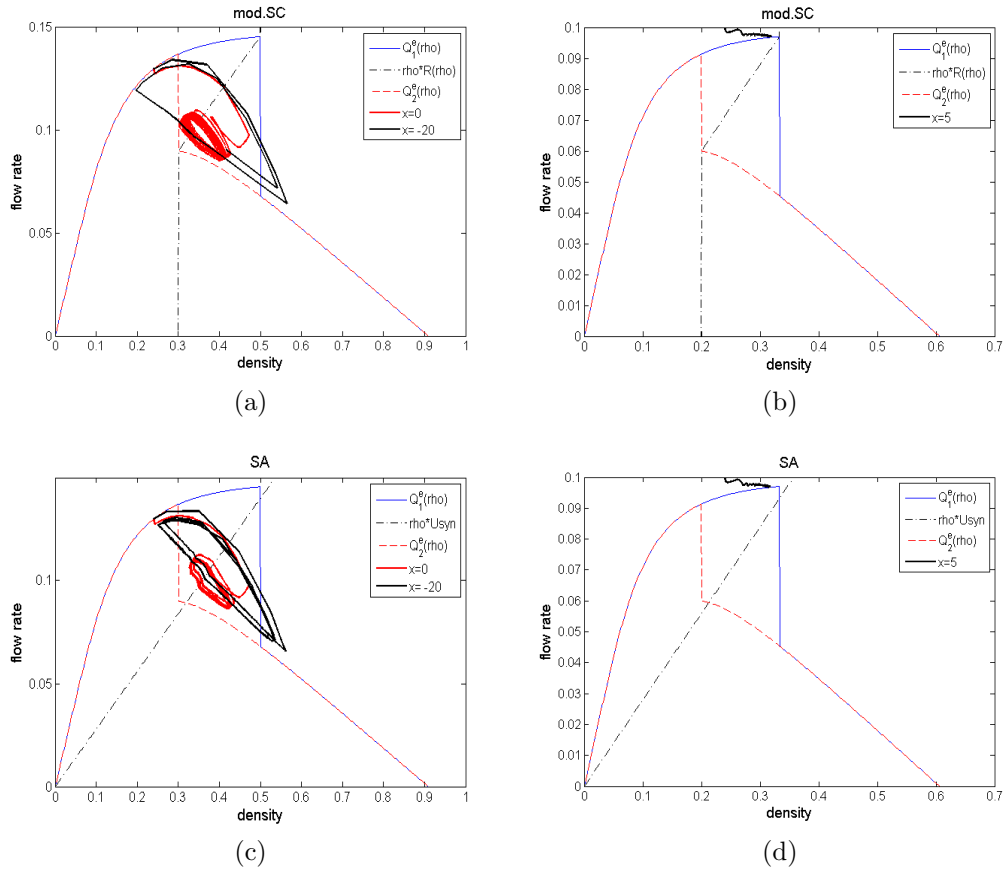

Figure 4.13: $\rho u - \rho$ relation for the modified Switching Curve (mod.SC) and the macroscopic Speed Adaptation (SA) models upstream, $x = -20$, within, $x = 0$, and downstream, $x = 5$, of the lane-drop bottleneck, figure 4.4.

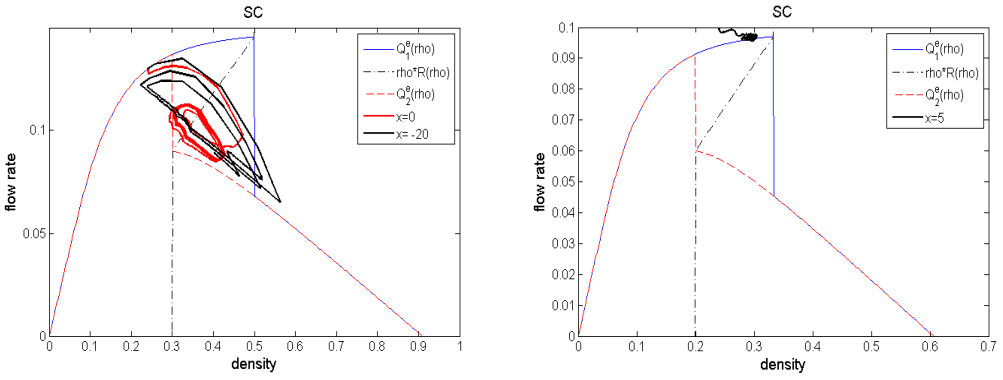

(a) (b)

Figure 4.14: $\rho u - \rho$ relation for the Switching Curve (SC) model upstream, $x = -20$, within, $x = 0$, and downstream, $x = 5$, of the lane-drop bottleneck, figure 4.4.

Remark 4.4.2. *Here we briefly report on the simulation results obtained by using the 'pressure law' $p_2(\rho) = V_{ref} ln(\frac{\rho}{\rho_{jam}})$ in the conservative system (3.68)-(3.69), with the relaxation term included, by comparing them with those reproduced by the same system but now with 'pressure law' $p_1(\rho) = C ln(\frac{\rho}{1-\rho})$. We take the constant $V_{ref} = 0.45$ and C is as given in table 4.1. In as far as the reproduction of spatiotemporal congested traffic patterns is concerned, the two 'pressure laws' yields qualitatively the same patterns as shown in figure 4.15. However, the jams propagate upstream at different speeds as shown in table 4.2, where we have used a maximal free flow velocity of 120 km/h. Also, as shown in figure 4.16, the density inside the jams is higher for the 'pressure law' p_2 than that of p_1; since $p_2(\rho) \leq p_1(\rho)$.*

Table 4.2: Wide moving jams propagation velocities in km/h.

	SC	*mod.SC*	*SA*
p_1	-23.9012	-22.2776	-28.7576
p_2	-23.4494	-22.0800	-25.4118

4.4.3 Simulation of Moving Bottlenecks

In vehicular traffic theory, a moving bottleneck on a multilane highway is usually a result of the slow motion of some vehicles such as trucks or buses. Numerous studies of moving bottlenecks with models within the fundamental diagram approach have been done. To mention a few, we state that the problem of moving bottleneck

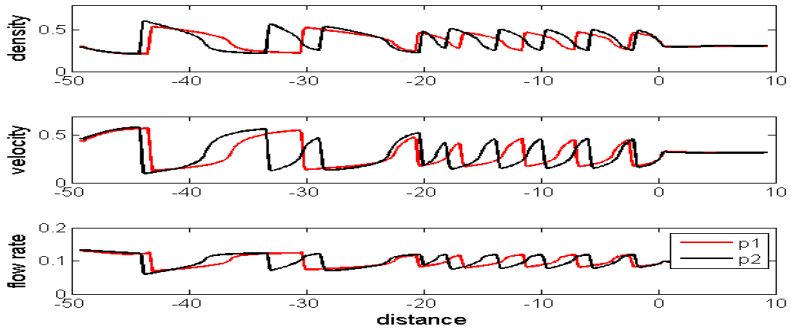

(a)

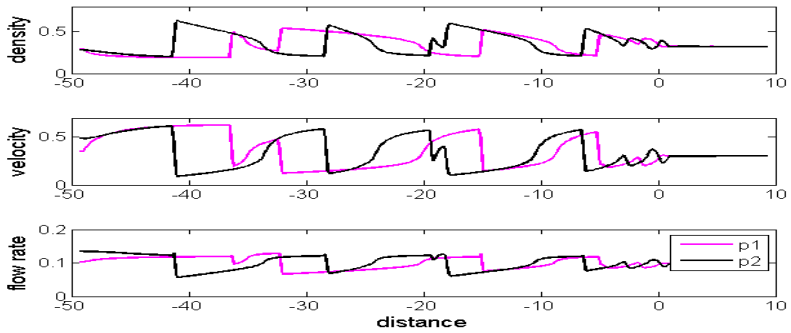

(b)

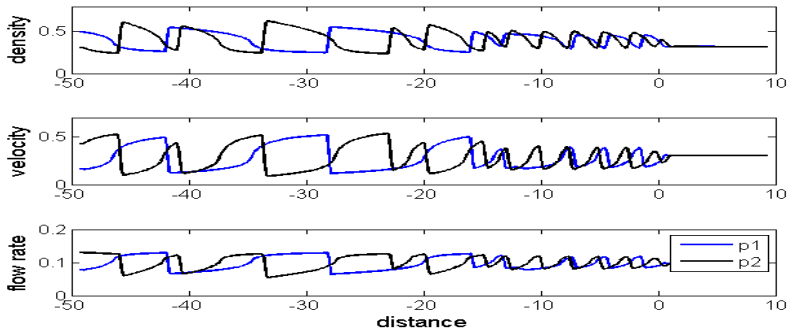

(c)

Figure 4.15: A comparison of simulation results of the Switching Curve (SC), modified Switching Curve (mod.SC) and macroscopic Speed Adaptation (SA) models, respectively, for the given 'pressure laws' p_1 and p_2. In (a)-(c), the results for $t = 400$ are displayed.

was introduced by Gazis and Herman [33] whereby they principally assumed that the discharge flow rate i.e. the flow rate just downstream of the moving bottleneck

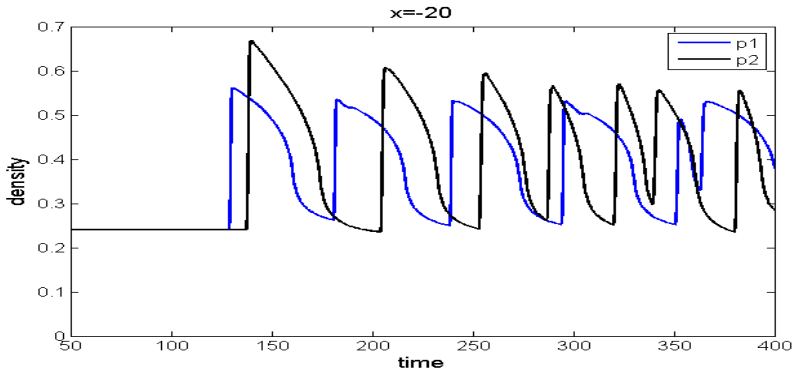

Figure 4.16: A comparison of density profiles of the macroscopic Speed Adaptation (SA) model for the given 'pressure laws' p_1 and p_2. We show the difference in density within the jams at distance $x = -20$, in figure 4.15.

is fixed. However, for all feasible bottleneck velocities this assumption is unrealistic. Newell [34] removed the above stated assumption of the discharge flow rate by suggesting that on say a 2-lane road the moving bottleneck is a long convoy such that the traffic stream in the lane adjacent to this long convoy can be represented on the flow-density plane by a scaled-down curve of the fundamental diagram of the 2-lane traffic flow. Thus enabling the discharge flow rate to vary, as shown in figure 3 of [34]. However, this model's prediction is that the discharge flow rate decreases with an increase in the moving bottleneck velocity. This is in contrast to empirical observations especially if the moving bottleneck is not necessarily a long convoy of vehicles as shown by Muñoz and Daganzo in [36], through experiments using the kinematic wave theory, that the discharge flow rate increases as the bottleneck velocity increases. Moreover, Kerner and Klenov [35] have recently studied the features of traffic breakdown of a moving bottleneck and the resulting spatial temporal congested patterns using the stochastic 3-phase traffic flow model [25]. It was observed that traffic breakdown is associated with the $F \to S$ phase transition and most of resulting congested patterns are qualitatively different from those arising from traffic congestion at motionless bottlenecks such as on/off-ramps and lane-drops. Now utilizing the relaxation term we demonstrate the ability of the Switching Curve, modified Switching Curve and the macroscopic Speed Adaptation models to reproduce the spontaneous emergence of congested traffic patterns at moving bottlenecks. Similar to the scaling of density that was done for the lane-drop bottleneck, we hereby achieve the effects of a moving bottleneck by scaling ρ in the relaxation terms (3.15), (3.56) and (3.59) by a function $\beta = \beta(x(t))$ as follows;

$$R(u, \rho, \beta) \quad = \quad \frac{1}{T}(U^e(\beta\rho, u) - u) \tag{4.28}$$

where β represents the change in traffic density due to the presence of a slow-moving vehicle platoon and satisfy the following, for the initial time $t = 0$:

(a) $1 \leq |\beta(x)| \leq \eta$ for any $x \in [-30, 30]$.

(b) $\beta(x) = 1$ in $(-30, -x_1) \cup (x_3, 30)$.

(c) $\beta(x) = \eta$ in $(0, x_2)$.

(d) $\beta(x)$ increases on $(-x_1, 0)$ and decreases on (x_2, x_3) with $x_2 - x_2 = |x_1|$.

as depicted in figure 4.17. Since this bottleneck is moving, we let the moving bot-

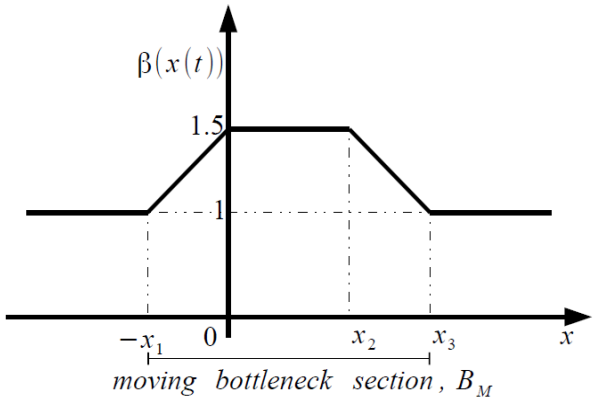

Figure 4.17: Function $\beta(x(t))$ at the initial time $t = 0$, with $\eta = 3/2$

tleneck section,B_M move on the outer lane of the considered 3-lane highway(figure 4.4,but without the lane-drop) at a constant velocity v_B, that can be any value less than the minimum possible velocity for free flow existence. This moving bottleneck section comprises of the length of the moving bottleneck, flanked on the rear and front sides by lane-changing sections for the faster vehicles. Now let $x_B(t)$ be the location of the moving bottleneck at time $t \in \mathbb{R}^+$. Then $x_B(t)$ is required to solve the ordinary differential equation;

$$\begin{cases} \dfrac{dx_B(t)}{dt} = v_B, \\ x_B(0) = x^0, \end{cases} \tag{4.29}$$

which describes the motion of the bottleneck along the highway. x^0 stands for the initial position of the bottleneck. Note that due to (4.29) also $x_1(t)$, $x_2(t)$, $x_3(t)$ will move at the same constant velocity v_B and the shape of $\beta(x(t))$ remains the same. Equation (4.29) is coupled with the traffic flow model equations to simulate the effects of the moving bottleneck on traffic flow on a multilane road. We choose the flow rate, ρu, great enough i.e. $\rho = 0.35$ and the velocity is given by $u = u_1^e(\rho)$

and vary the moving bottleneck velocity v_B as 0.1, 0.17. Moreover, we choose the initial positions of the bottleneck section as $x_1 = -1,\ x_2 = 3,\ x_3 = 4$. It is clear that faster vehicles will have all the intentions to pass the slow-moving vehicle/platoon by changing lanes to the adjacent lanes. This vehicle lane changing maneuvres that occurs within the rear lane-changing section of the moving bottleneck causes a deterministic velocity disturbance that moves at the velocity v_B and is localized at the moving bottleneck. If the moving bottleneck velocity is relatively low i.e $v_B = 0.1$ and the flow rate on the multilane road is great enough, traffic breakdown spontaneously appear within the deterministic disturbance at the moving bottleneck and as a result narrow moving jams will appear in the case of the macroscopic 3-phase traffic flow models: macroscopic Speed Adaptation (SA) model and modified Switching Curve (mod.SC) model, figure 4.18. The Switching Curve (SC) model, in the same figure 4.18, also predicts the spontaneous emergence of moving jams within the moving deterministic disturbance at the moving bottleneck. But these jams have a greater width as compared to those of the SA and mod.SC models. In the three cases, we observe that the emergence of the wide moving jams suppresses the growth of the smaller jams leading to their dissolution.

At higher bottleneck velocity $v_B = 0.17$, see figure 4.19, we observe a different behavior of traffic flow predicted by the three models. Basically, there is the formation of wide moving jams separated by widening synchronized flow (WSP) in the vicinity of the moving bottleneck. The WSP is usually a congested traffic pattern of high velocity and less density compared to other congested traffic patterns, that are feasible once traffic breakdown has occurred at a bottleneck. The number of wide moving jams formed in the mod.SC model is significantly less compared to the other two models. While traffic congests upstream of the moving bottleneck, free flow is realized downstream of this bottleneck as clearly depicted in the figures 4.18 and 4.19. Although it is not shown here, for a bottleneck moving at velocity $v_B = 0.2$, only WSP formed upstream of the moving bottleneck. If v_B takes much higher values, then there will be hardly any congested pattern formation upstream of the moving bottleneck and consequently the flow rate downstream of the bottleneck will remain high and within the range of the initial value, that was chosen great enough. Hence we can conclude that an increase of the moving bottleneck velocity, v_B is accompanied by an increase in the flow rate just downstream of this moving bottleneck i.e. an increase of the discharge flow rate, as was empirically observed by Muñoz and Daganzo in [36].

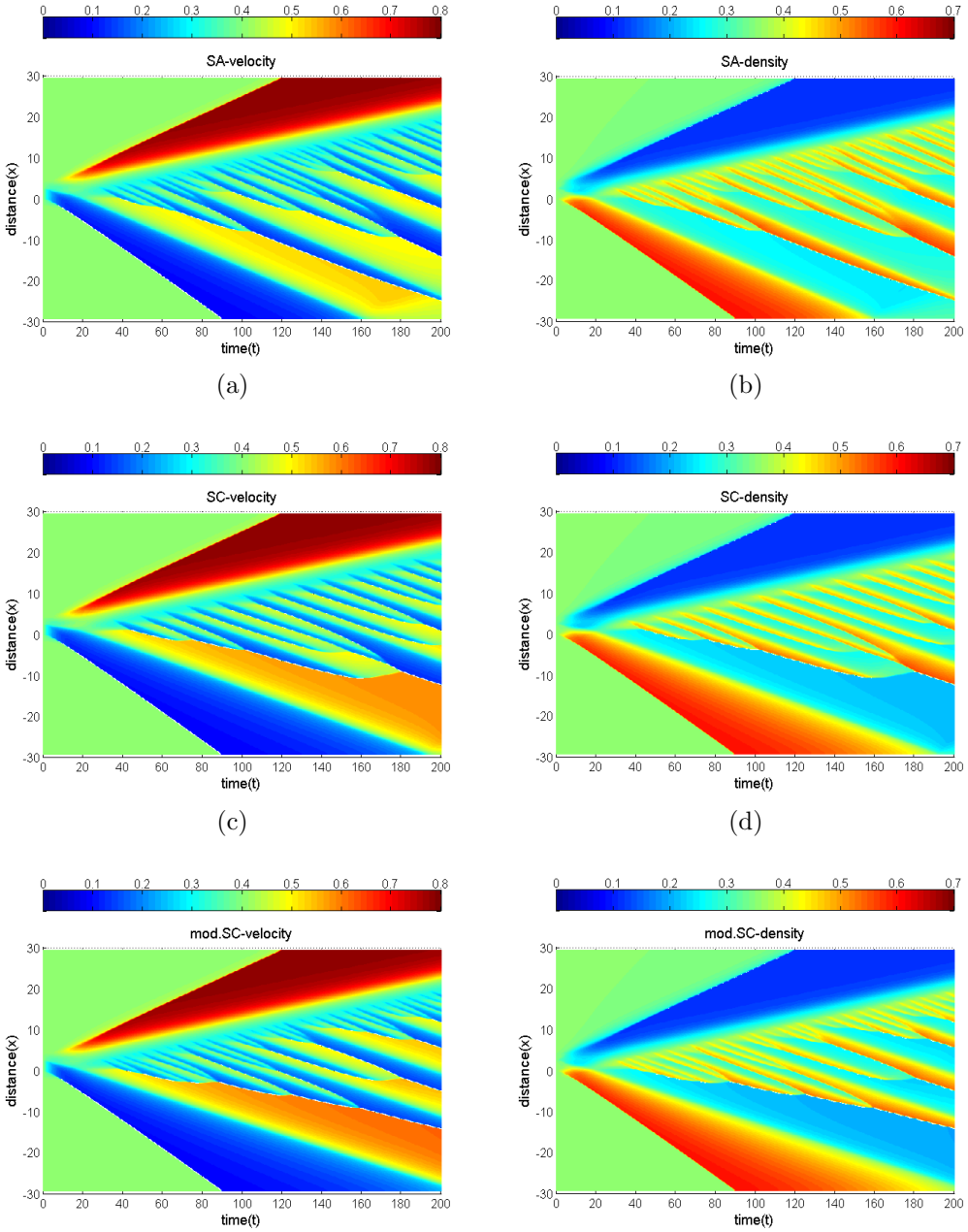

Figure 4.18: Spatiotemporal congested traffic patterns caused by a bottleneck moving at $v_B = 0.1$

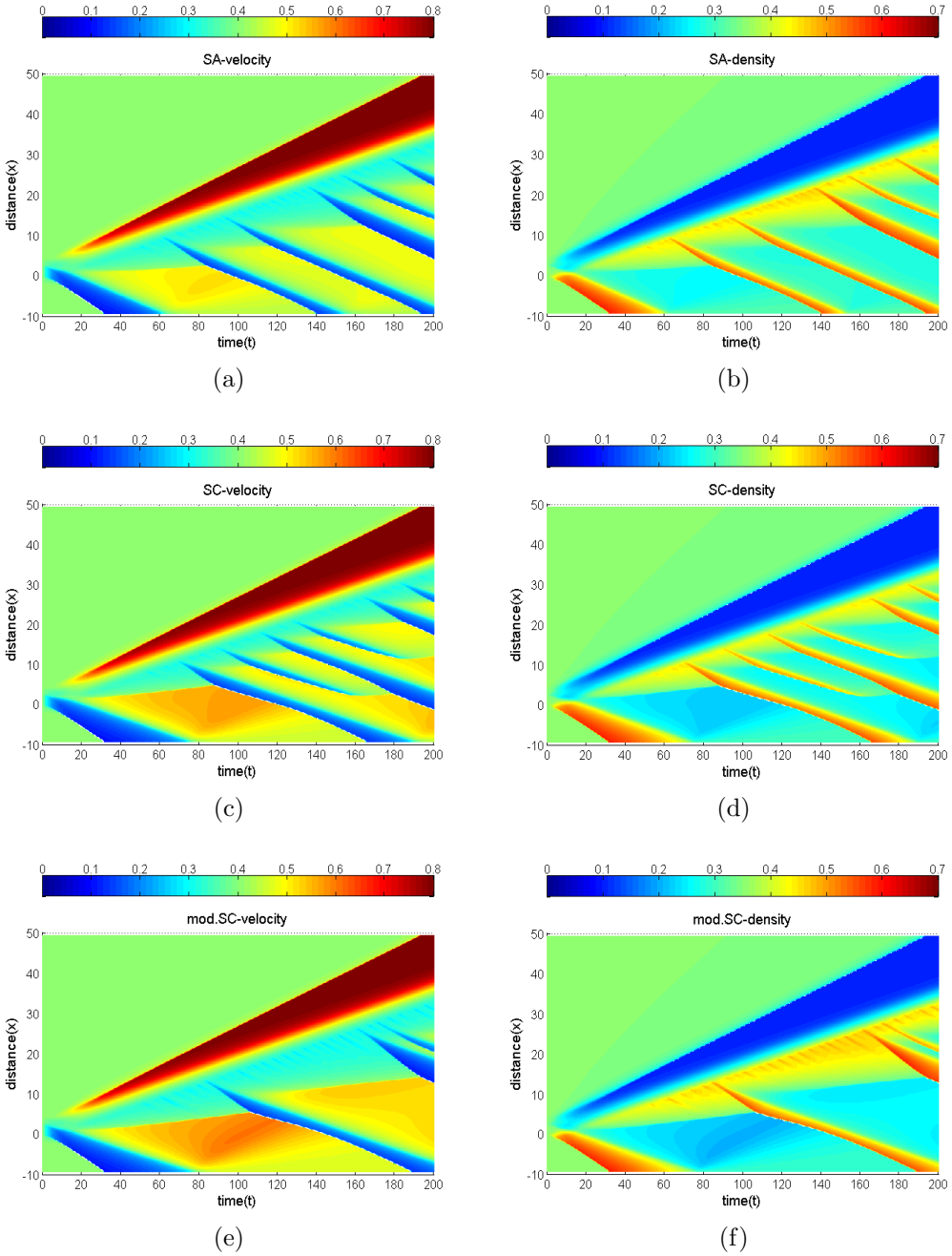

Figure 4.19: Spatiotemporal congested traffic patterns caused by a bottleneck moving at $v_B = 0.17$

Conclusion

In this study macroscopic traffic flow models within the framework of Kerner's 3-phase traffic flow theory have been presented. The 3-phase traffic theory is constituted in the macroscopic equations through the relaxation term. The idea is to preserve the 2D region of steady states of synchronized flow by introducing two density-dependent optimal velocity curves which satisfy certain properties for the given density ranges. It is the difference in these properties that brings about three kinds of relaxation terms that in turn result in three kinds of macroscopic traffic models. The macroscopic model equations, which are of the Aw-Rascle type, are derived from microscopic and kinetic traffic models. We use transformation of coordinates from Lagrangian to Eulerian in order to obtain the macroscopic model equations from the microscopic equations. As for the derivation from kinetic models, we use a one-node quadrature ansatz [10, 11] to obtain Aw-Rascle type model equations from kinetic models based on integro-differential equations and on the Fokker-Planck type of equations. The hyperbolic nature of the derived macroscopic models is studied. By construction of the solutions to the Riemann problem, set up using the conservative form of the model, the model features have been explored further. The numerical method for solving the macroscopic model in conservative form is discussed and tests are carried out to show the effectiveness of the numerical method used. Using this numerical method we go ahead to simulate traffic flow on a roadway with a lane-drop bottleneck and a moving bottleneck. Through these simulations, we assess the ability of the derived macroscopic traffic flow models i.e. the Switching Curve, modified Switching Curve and macroscopic Speed Adaptation models to reproduce the complex spatiotemporal features of traffic flow. Namely the first order $F \to S$ transition and the coexistence of free flow (F), synchronized flow (S) and wide moving jams (J) as observed in real traffic flow. We state here that empirical investigation, see for instance [32] indicate that unless synchronized flow is hindered, moving jams do not emerge in free flow but rather emerge in the synchronized flow phase of traffic. That is their emergence is due to a sequence of two first order phase transitions: $F \to S$ and $S \to J$. This is because the onset of congestion in an initial free flowing traffic is associated with $F \to S$ transition and later on at some location upstream of the bottleneck, $S \to J$ transition occurs depending on the bottleneck strength and the traffic demand. Generally, of the three models investigated, the macroscopic Speed Adaptation and modified Switching Curve model gives better prediction of 3-phase traffic theory principle than the Switching Curve model.

Bibliography

[1] B.S. Kerner, Introduction to modern traffic flow theory and control: The long road to three-phase traffic theory, *Springer, 1st Edition*, 2009.

[2] A. Aw, A. Klar,A. Materne,M. Rascle, Derivation of continuum traffic flow models from microscopic follow-the-leader models, *SIAM J. Appl. Math., Vol.63 No.1, pp.259–278*, 2002.

[3] B.S. Kerner and S.Klenov, Deterministic microscopic three-phase traffic flow models, *J. Phys. A: Math. Gen. Vol.39 No.8, pp.1775-1810*, 2006.

[4] D. Helbing, Gas-kinetic derivation of Navier-Stokes-like traffic equations, *Phys. Rev. E, Vol.53 No.3, pp.2366-2381*, 1996.

[5] D. Helbing, Derivation and empirical validation of a refined traffic flow model, *Physica A, 233, pp.253-282*, 1996.

[6] A. Klar and R. Wegener, Kinetic derivation of macroscopic anticipation models for vehicular traffic, *SIAM J. Appl. Math., Vol.60 No.5, pp.1749-1766*, 2000.

[7] V. Shvetsov and D. Helbing, Macroscopic dynamics of multilane traffic, *Phys. Rev. E, Vol.59 No.6, pp.6328-6339*, 1999.

[8] A. Aw and M. Rascle, Resurrection of "second-order" models of traffic flow, *SIAM J. Appl. Math., Vol.60 No.3, pp.916-938*, 2000.

[9] C. F. Daganzo, Requiem for second-order fluid approximations of traffic flow, *Trans. Res., Part B, Vol.29 No.4, pp.277-286*, 1995.

[10] D. L. Marchisio, R.D. Vigil, R.O. Fox, Quadrature method of moments for aggregation-breakage processes, *J. Colloid Int. Sci., 258, pp.322-334* , 2003.

[11] O. Desjardins, R.O. Fox, P. Villedieu, A quadrature-based moment method for dilute fluid-particle flows, *J. Comput. Phys., 227, pp.2514-2539* , 2008.

[12] R. Illner, C. Stoica, A. Klar, R. Wegener, Kinetic equilibria in traffic flow models, *Trans. Theory and Statist. Phys., Vol.31, No.7, pp.615-634* , 2002.

[13] D. Helbing, A.F. Johansson, On the controversy around Daganzo's requiem for and Aw-Rascle's resurrection of second-order traffic flow models, *European Physical Journal B Vol.69, No.4, pp.549-562* , 2009.

[14] J.M. Greenberg, A. Klar, M. Rascle, Congestion on multilane highways, *SIAM J. Appl. Math., Vol.63, No.3, pp.818-833* , 2003.

[15] P.D. Lax, Hyperbolic systems of conservation laws and the mathematical theory of shock waves, *SIAM Regional Conference Series in Applied Mathematics, No.11* , 1972.

[16] C. Chalons and P. Goatin, Transport-equilibrium schemes for computing contact discontinuities in traffic flow modeling, *Commun. Math. Sci., Vol.5, No.3, pp.533-551* , 2007.

[17] R.J. LeVeque, Numerical methods for conservation laws, *Birkhaeuser Basel, 2nd Edition* , 2005.

[18] C. Chalons and P. Goatin, Godunov scheme and sampling technique for computing phase transitions in traffic flow modeling, *Interfaces and Free Boundaries, Vol.10, No.2* , 2008.

[19] B.S. Kerner, Three-phase traffic theory and highway capacity, *Physica A: Statist. Theor. Phys., Vol.333, pp.379-440*, 2004.

[20] H. Rehborn, S.L. Klenov and J.Palmer, Common traffic congestion features studied in USA,UK, and Germany employing Kerner's three-phase traffic theory, *arXiv:1012.5160v1*, 2010.

[21] M. Schoehof and D.Helbing, Criticism of three-phase traffic theory, *Trans. Res., Part B, Vol.43 No.7, pp.784-797*, 2009.

[22] D.P. Sullivan and R.J.Troutbeck, The use of Cowan's M3 headway distribution for modeling urban traffic flow, *Traffic Eng. Contr., Vol.35 No.7-8, pp.445-450*, 1994.

[23] B.S. Kerner, A theory of traffic congestion at heavy bottlenecks, *J. Phys. A: Math. Theor., Vol.41, 215101* , 2008.

[24] B.S. Kerner, Experimental features of self-organization in traffic flow, *Phys. Rev. Lett., Vol.81 No.17, pp.3797-3800* , 1998.

[25] B.S. Kerner and S.L. Klenov, Microscopic theory of spatial-temporal congested patterns at highway bottlenecks, *Phys. Rev. E, Vol.68, 036130* , 2003.

[26] B.S. Kerner, S.L. Klenov, D.E. Wolf, Cellular automata approach to three-phase traffic theory, *J. Phys. A: Math. Gen., Vol.35, pp.9971-10013* , 2002.

[27] K. Gao, R. Jiang, S-X. Hu, B-H. Wang, Q.S. Wu, Cellular-automata model with velocity adaptation in the framework of Kerner's three-phase traffic theory, *Phys. Rev. E, Vol.76, 026105* , 2007.

[28] M. Treiber, A. Kesting, D. Helbing, Three-phase traffic theory and two-phase models with a fundamental diagram in the light of empirical stylized facts, *Trans. Res., Part B Vol.44, pp.983-1000* , 2010.

[29] P. Collela, Glimm's method for gas dynamics, *SIAM J. Sci. Stat. Comput. 3, pp.76-110* , 1982.

[30] E.F. Toro, Riemann solvers and numerical methods for fluid dynamics: A practical introduction, *Springer; 3rd Edition* , 2009.

[31] B.S. Kerner, Dependence of empirical fundamental diagram on spatial-temporal traffic patterns features, *arXiv:cond-mat/0309018v1*, 2003.

[32] B.S. Kerner, Empirical macroscopic features of spatial-temporal traffic patterns at highway bottlenecks, *Phys. Rev. E, Vol.65, 046138* , 2002.

[33] D.C. Gazis, R. Hermann, The moving and 'phantom' bottlenecks, *Trans. Sci., Vol.26 No.3, pp.223-229* , 1992.

[34] G.F. Newell, A moving bottleneck, *Trans. Res. Part B, Vol.32 No.8, pp.531-537* , 1998.

[35] B.S. Kerner, S.L. Klenov, A theory of traffic congestion at moving bottlenecks, *J. Phys. A: Math. Theor., Vol.43, 425101*, 2010.

[36] J.C. Muñoz, C.F. Daganzo, Moving bottlenecks: A theory grounded on experimental observation, *In 15th Int. Symp. on Trans. and Traffic Theory(M.A.P. Taylor,ed.), Pergamon-Elsevier, Oxford, UK, pp.441-462* , 2002.

[37] M. Treiber, M. Hennecke, D. Helbing,,Derivation, properties, and simulation of a gas-kinetic-based, non-local traffic model, *Phys. Rev. E Vol.59 No.1, pp.239253*, 1999.

[38] R. Illner, A. Klar, T. Materne, Vlasov-Fokker-Planck models for multilane traffic flow, *Comm. Math. Sci., Vol.1, No.1, pp.1-12* , 2003.

[39] S.P. Hoogendoorn, Multiclass continuum modelling of multilane traffic flow, *Ph.D. Thesis, Delft University of Technology, Netherlands*, 1999.

[40] R. Borsche, M. Kimathi, A. Klar, Kinetic derivations of a Hamilton-Jacobi type traffic flow model, *submitted.*

[41] R. Borsche, M. Kimathi, A. Klar, A comparison of multiphase traffic theories for microscopic, kinetic and continuum traffic flow models, *submitted.*

List of Figures

List of Tables